Figure 5
LICs have higher proteasome activity than non-LICs. (**A** and **B**) Immunoblotting of IκBα in LICs and non-LICs (**A**). Protein levels were quantified with ImageJ software (**B**). Data representative of four experiments with SD are shown. (**C**) Relative mRNA expression of *Nfkbia* in LICs compared with that in non-LICs ($n = 4$ each). Error bars indicate SD. (**D** and **E**) Immunoblotting of IκBα in LICs and non-LICs. Cells were pretreated with MG132 for 1 hour and incubated for an additional hour with or without cycloheximide (CHX) (**D**). IκBα protein levels were quantified with ImageJ software, and the relative decrease in IκBα after cycloheximide treatment was calculated ($n = 3$ each). Error bars indicate SD (**E**). (**F**) Analysis of 20S proteasome activity quantified with fluorescence produced upon cleavage of the proteasome substrate SUC-LLVY-AMC ($n = 4$ each). Error bars indicate SD. (**G**) Relative mRNA expression of proteasome subunits in LICs compared with that in non-LICs ($n = 4$ each). Error bars indicate SD. (**H**) Schematic representation of the experiments. Each type of LIC was secondarily transplanted into mice. Bortezomib was injected twice weekly or injected once after incidence of leukemia. (**I** and **J**) Comparison of surface marker profiles in leukemic mice treated with bortezomib or vehicle. Representative FACS data (**I**) and relative percentages of Gr-1^{lo} c-Kit^{hi} fraction in MLL-ENL– or MOZ-TIF2–induced leukemic mice, and Gr-1^{lo}Sca-1^{hi} fraction in BCR-ABL/NUP98-HOXA9–induced leukemic mice are shown ($n = 3$ each) (**J**). Values of control mice were normalized to 100%. Error bars indicate SD. (**K**) Survival curves of mice in the experiments shown in **H** ($n = 6$ each).

progression. Unveiling the role of TNF-α as a paracrine mediator would further extend the therapeutic options for AML.

Few studies have compared the NF-κB activity of different fractions within leukemia cells, and the mechanism underlying the difference in this activity has not been analyzed (44). We focused on proteasome activity as the essential machinery supporting NF-κB activity in LICs. Although high proteasome activity has been reported in various types of cancers (45, 46), its actual role in the malignant phenotype remained to be elucidated. In this study, we found that proteasome activity was especially high in LICs, which contributed to selective NF-κB activity in LICs via the efficient degradation of IκBα. Conversely, the inefficient NF-κB nuclear translocation we observed in non-LICs, despite TNF-α–enriched leukemic BM cells, could be explained by the low proteasome activity in these cells. Therefore, we postulate that both an activating stimulus such as TNF-α and high proteasome activity are required for efficient NF-κB signaling (Figure 7F). Both of these conditions are present exclusively in LICs, which acquire selective NF-κB activation. We also found that the expression levels of proteasome subunit genes were elevated in LICs compared with those in non-LICs, genes that could be involved in regulating proteasome function. Because we observed similar expression patterns in LICs and non-LICs in human AML cells, an elevated expression level of proteosome subunit genes might be one of the common characteristics of the LIC phenotype. Further studies will be needed to elucidate the regulatory mechanism of the proteasome gene families.

Our findings provide several advantages when considering their application to the clinical care setting. First, an activated NF-κB/TNF-α feedback loop was seen in AML LICs that had different genetic abnormalities. Although the therapeutic strategy of targeting aberrant molecules based on genetic abnormalities such as FLT3-ITD is promising, its application is limited to a particular group of patients. In contrast, inhibition of the NF-κB signal in addition to standard chemotherapy would show beneficial effects in most AML patients. Second, because there was a strong positive correlation between the NF-κB signal and TNF-α secretion, therapeutic efficacy could easily be inferred from the abundance of TNF-α instead of from evaluation of the activation status of NF-κB. Third, the NF-κB/TNF-α signal and enhanced proteasome activity are selectively seen in LICs, but not in normal HSCs. A recent study has shown that complete ablation of p65 in hematopoietic cells attenuates the long-term capacity for hematopoietic reconstitution (47). However, our data from the experiments in which we introduced IκB-SR into normal BM cells show that partial repression of NF-κB activity exerted minimal influence on normal hematopoiesis, while it markedly inhibited leukemia progression. These results indicate that there is a therapeutic window during which LICs can selectively be killed by NF-κB inhibition without seriously affecting normal hematopoiesis. Alternatively, there is some evidence that TNF-α has suppressive effects on normal HSCs (48, 49). The opposing role of TNF-α in LICs and HSCs is additionally beneficial, since anti–TNF-α therapy contributes to the recovery of normal hematopoiesis and attenuates LIC proliferation. Now that the TNF-α antagonist etanercept is widely used in inflammatory diseases such as rheumatoid arthritis, this drug might be a promising candidate for treating patients with AML.

In summary, the present study shows that blocking the NF-κB pathway offers a promising therapeutic approach for targeting LICs in various types of myeloid leukemia, without disturbing normal hematopoiesis. We further determined that autocrine TNF-α signaling and enhanced proteasome activity are crucial for maintaining constitutive NF-κB activity in LICs, findings that may also provide a new therapeutic opportunity.

Methods

Animals. C57BL/6 mice and BALB/c mice were purchased from Japan SLC, Inc. *Tnf*-knockout mice on a BALB/c background were established as described previously (50). *Rela*-floxed mice on a C57BL/6 background were provided by H. Algül and R.M. Schmid (32). BALB/c mice were used as the controls in the experiments using *Tnf*-knockout mice, and C57BL/6 mice were used in the other experiments.

Retrovirus production and BM transplantation assays. To obtain retrovirus supernatants, platinum-E (Plat-E) packaging cells were transiently transfected with each retrovirus vector, and the viral supernatants were collected 48 hours after transfection and used immediately for infection. To establish each myeloid leukemia mouse model, we used pMSCV-neo-MLL-ENL; pMSCV-MLL-ENL–internal ribosome entry site–*EGFP* (*IRES-EGFP*); pGCDNsam-MLL-ENL-*IRES*-Kusabira-Orange; pGCDNsam-MOZ-TIF2-*IRES-EGFP*; pGCDNsam-MOZ-TIF2-*IRES*-Kusabira-Orange; pGCDNsam-BCR-ABL-*IRES-EGFP*; pGCDNsam-BCR-ABL-*IRES*-Kusabira-Orange; and pMSCV-neo-NUP98-HOXA9. GMPs isolated from the BM of 8- to 10-week-old mice were transduced with the respective vectors and injected into sublethally irradiated (7.5 Gy) recipient mice. For experiments involving the generation of leukemia cells with IκB-SR, MLL-ENL leukemia cells were transduced with pBabe-GFP or pBabe-GFP-IκB-SR. MOZ-TIF2, and BCR-ABL/NUP98-HOXA9 leukemia cells were transduced with pGCDNsam-Kusabira-Orange or pGCDNsam-IκB-SR-IRES-Kusabira-Orange. For experiments involving the deletion of p65 in *Rela*-floxed mice, leukemia cells were established using Kusabira-Orange–containing retroviral vectors. The developed leukemia cells were transduced with pGCDNsam-EGFP or pGCDNsam-iCre-EGFP and transplanted into sublethally irradiated mice.

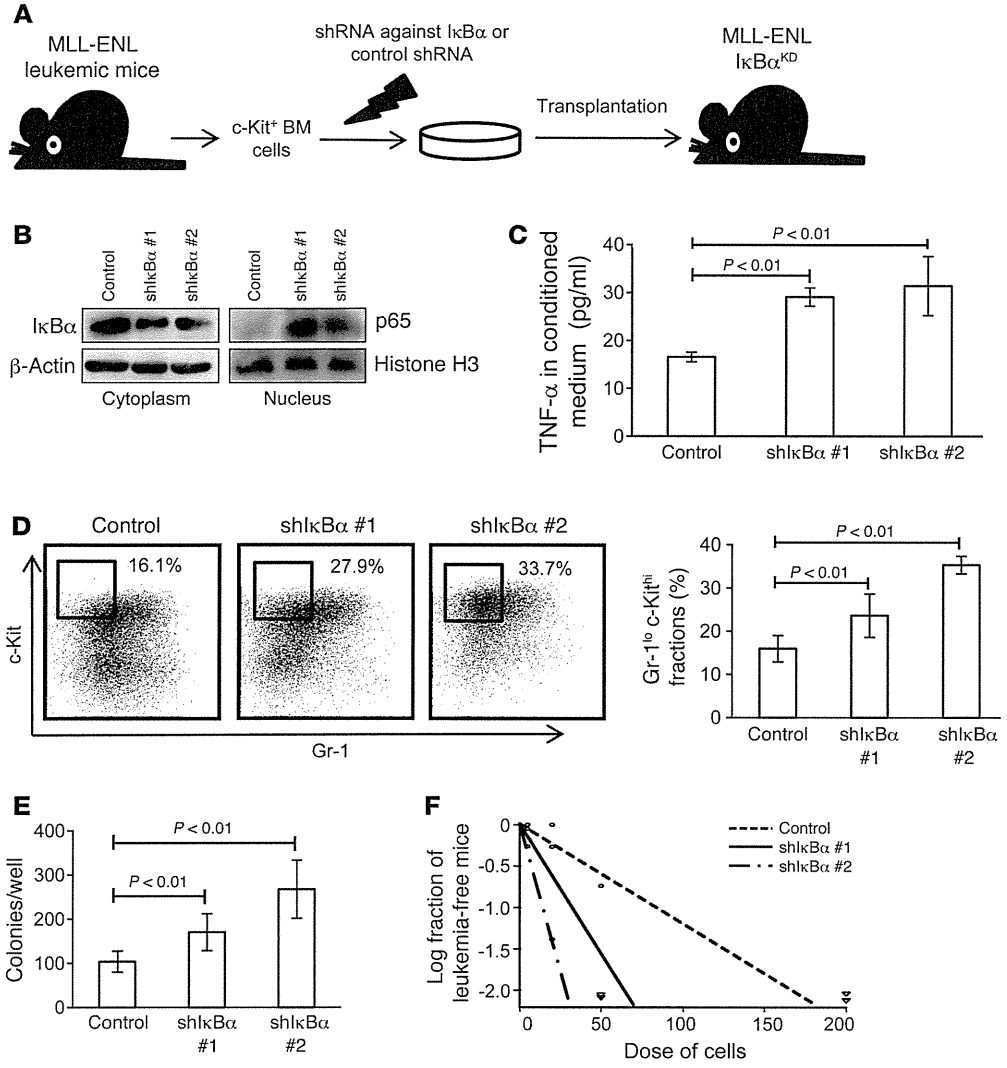

Figure 6
Forcible maintenance of NF-κB activity in leukemia cells enhances LIC frequency. (**A**) Schematic representation of the experiments. c-Kit+ BM cells isolated from MLL-ENL leukemic mice were transduced with shRNA against IκBα or control shRNA and transplanted into sublethally irradiated mice. (**B**) Immunoblotting of cytoplasmic IκBα and nuclear p65 in BM mononuclear cells from MLL-ENL-IκBα^{KD} mice compared with those from control leukemic mice. (**C**) TNF-α secretory ability of MLL-ENL-IκBα^{KD} leukemia cells compared with that of control leukemia cells (n = 4 each). Error bars indicate SD. (**D**) Surface marker profiles of MLL-ENL leukemic mice with or without knockdown of IκBα. Representative FACS plots and mean percentages of Gr-1^{lo}c-Kit^{hi} fractions (n = 6 each). (**E**) CFC assay of MLL-ENL leukemia cells with or without knockdown of IκBα (n = 6). Cells were seeded at 500 cells per well. Error bars indicate SD. (**F**) LIC frequency in BM mononuclear cells derived from MLL-ENL-IκBα^{KD} leukemic mice compared with those from control mice as determined by limiting dilution transplantation assay.

In vivo limiting dilution assays. Varying numbers of cells from different populations were transplanted into sublethally irradiated mice and monitored for disease development (see Supplemental Table 1 for the injected cell numbers).

Immunofluorescence and quantification of p65 nuclear translocation. A total of 1 × 10^4 to 5 × 10^4 cells were cytospun onto glass slides. The cells were fixed with 3.7% formaldehyde in PBS for 30 minutes, permeabilized by treatment with 0.2% Triton X in PBS for 10 minutes, and blocked with 1% BSA in PBS for 60 minutes. Then, the slides were incubated with rabbit anti–p65 polyclonal antibody (sc-372; 1:100 dilution; Santa Cruz Biotechnology Inc.) overnight at 4°C, followed by incubation with Alexa Fluor 555 goat anti-mouse IgG (1:250 dilution; Invitrogen) and TO-PRO3 (1:1,000 dilution; Invitrogen) for 90 minutes. For immunofluorescence staining of Kusabira-Orange$^+$ leukemia cells, Alexa Fluor 647 goat anti-mouse IgG (1:250 dilution; Invitrogen) was used as a secondary antibody, and the nucleus was stained with DAPI. After the cells were washed, they were treated with ProLong Gold Antifade Reagent (Invitrogen). Images were acquired using an Olympus FluoView FV10i confocal microscope with a ×60 objective oil immersion lens. The mean intensity of p65 in the nucleus and cytoplasm of each cell was measured within a region of interest (ROI) placed within the nucleus and cytoplasm. Similarly, the background intensity was quantified within an ROI placed outside the cells. All the measurements were performed using FluoView software. The background-subtracted intensity ratio of nucleus/cytoplasm was calculated in more than 50 cells in each specimen, and the average intensity with SD is presented.

Flow cytometry. Isolation of each fraction from normal or leukemic BM cells was performed using a FACSAria II (BD) cell sorter. For isolation of GMPs and KSLs, biotinylated antibodies against Gr-1 (RB6-8C5), CD11b (M1/70), B220 (RA-3-6B2), CD3 (145-2C11), CD4 (GK1.5), CD8 (53-6.7), and TER119 were used for lineage staining. A PerCP-Cy5.5–labeled streptavidin antibody was used for secondary staining, together with APC-anti–c-Kit (2B8), PE-Cy7–anti-Sca-1 (E13-161.7). FITC-anti-CD34 (RAM34), and PE-anti-CD16/32b antibodies (clone 93). The following antibodies were used for isolation of L-GMPs from GFP-containing leukemia cells: APC-Cy7–anti-streptavidin, PE-Cy5–anti–c-Kit (2B8), PE-Cy7–anti-Sca-1 (E13-161.7), Alexa Fluor 647–anti-CD34 (RAM34), and PE–anti-CD16/32b (clone 93). APC-antistreptavidin and PE-Cy7–anti-Sca-1 antibodies (E13-161.7) were used for sorting LICs and non-LICs in the BCR-ABL plus NUP98-HOXA9 leukemia model. See Supplemental Figures 1 and 2 for detailed FACS plots. For analysis of TNF receptor expression in leukemia cells, biotinylated antibodies against TNF receptor I or II (55R-170) and an APC-Cy7–antistreptavidin antibody were used. Analysis was performed using FlowJo software (Tree Star Inc.).

Table 1
Clinical characteristics of the 12 patients with AML and the 5 patients with normal BM findings

Patient no.	Age	Sex	BM findings	Disease status	Type	Cytogenetics	Blast (%)
1	42	M	AML	Untreated	M2	Normal	87
2	62	M	AML	Relapse	M1	47, XY, del(9)(q13q22),+10	96
3	69	M	AML	Untreated	M4	Normal	90
4	58	M	AML	Untreated	M3	46, XY, t(15;17)	63
5	75	M	AML	Untreated	M4	46, XY, inv(16)	27
6	62	F	AML	Untreated	AML-MRC	NA	24.8
7	72	F	AML	Untreated	AML-MRC	Complex	21
8	42	M	AML	Untreated	M4	46, XY, t(11;17)	25
9	66	M	AML	Untreated	M1	46, XY, t(8;21)	85.4
10	73	F	AML	Untreated	AML-MRC	Complex	44.5
11	65	M	AML	Untreated	AML-MRC	46, XY, t(1;3)	53.3
12	73	M	AML	Untreated	M2	46, XY, add(7)	51.5
13	67	F	Normal			Normal	
14	64	F	Normal			Normal	
15	47	F	Normal			Normal	
16	54	M	Normal			Normal	
17	29	M	Normal			Normal	

Real-time quantitative PCR. Real-time quantitative PCR was carried out on the LightCycler480 system (Roche) using SYBR green reagents according to the manufacturer's instructions. The results were normalized to *Gapdh* levels. Relative expression levels were calculated using the 2-ΔΔCt method (51). The following primers were used for real-time PCR experiments: *Gapdh* forward, TGGCCTCCAAGGAGTAAGAA, and reverse, GGTCTGGGATGGAAATTGTG; *Ncf2* forward, CCAGAAGACCTGGAATTTGTG, and reverse, AAATGCCAACTTTCCCTTTACA; *Tnf* forward, TCTTCTCATTCCTGCTTGTGG, and reverse, GGTCTGGGCCATAGAACTGA; *Il15ra* forward, TAAGCGGAAAGCTGGAACAT, and reverse, TGAGGTCACCTTTGGTGTCA; *Litaf* forward, CTCCAGGACCTTACCAAGCA, and reverse, AGGTGGATTCATTCCCTTCC; *Hoxa9* forward, GGTGCCTGCTGCAGTGTAT, and reverse, GTTCCAGCCAGGAGCGCATAT; *Psma5* forward, CGAGTACGACAGGGGTGTG, and reverse, TGGATGCCAATGGCTGTAG; *Psmd4* forward, GTACATGCGGAACGGAGACT, and reverse, TGTGGTCAGCACCTCACAGT; *Psme3* forward, TTTCAGAGAGCGGATCACAA, and reverse, GGTCATGGATATTTAGAATTGGTTC.

siRNA interference. Specific shRNAs targeting murine *Ikba* mRNA were designed and cloned into pSIREN-RetroQ-ZaGreen vectors. Control shRNA is a nonfunctional construct provided by Clontech. The target sequences, from 5′ to 3′, were: CCGAGACTTTCGAGGAAAT (shIκBα number 1), and AGCTGACCCTGGAAAATCT (shIκBα number. 2).

Immunoblotting. Membranes were probed with the following antibodies: anti-IκBα (Cell Signaling Technology), anti-phospho-IκBα (Ser32) (Cell Signaling Technology), anti-p65 (Santa Cruz Biotechnology Inc.), anti-phospho-p65 (Ser536) (Cell Signaling Technology), anti-β-actin (Cell Signaling Technology), and anti-histone H3 (Cell Signaling Technology). Protein levels were quantified with ImageJ software (NIH). To obtain nuclear and cytoplasmic extracts, an Active Motif Nuclear Extract Kit was used according to the manufacturer's instructions. Cycloheximide treatment assay was performed as described previously, with modification (52). Cells were pretreated with MG132 (20 μM) for 1 hour to initially inhibit the proteasomal degradation of IκBα. Cells were washed twice with medium, then cultured with or without 10 μg/ml of cycloheximide for an additional hour and harvested.

CFC assays. In each experiment, cells were plated onto MethoCult GF M3434 medium (STEMCELL Technologies). Colony numbers in each dish were scored on day 7.

Measurement of TNF-α levels in BM extracellular fluid and conditioned media. BM extracellular fluid was obtained by flushing bilateral femurs and tibia of individual mice with 400 μl PBS. The supernatant was collected after centrifugation. To obtain conditioned media, 0.3–1.0 × 10^6 murine leukemia cells or normal GMPs were cultured in RPMI medium containing 10% FBS and 10 ng/ml IL-3. After a 48-hour incubation, the culture supernatants were collected. The concentration of TNF-α was measured using a murine TNF-α ELISA kit (Gen-Probe Diaclone) according to the manufacturer's instructions. Similarly, 0.5 × 10^4 to 2.0 × 10^4 human AML or normal $CD34^+CD38^-$ cells were cultured for 48 hours in RPMI medium containing 10% FBS and 100 ng/ml SCF, IL-3, and thrombopoietin. The concentration of TNF-α in the harvested supernatants was measured with a human TNF-α Quantikine ELISA kit (R&D Systems).

20S proteasome activity. A 20S proteasome activity assay kit (Cayman Chemical) was used to analyze proteasome activity. A total of 5 × 10^4 freshly isolated normal GMPs, LICs, and non-LICs in each model were assayed according to the manufacturer's protocol. As a control, the proteasome activity of each cell was also assayed after the specific proteasome inhibitor epigallocatechin gallate was added. Fluorescence was measured with a Wallac ARVO V (PerkinElmer), and the proteasome activity of each cell type was calculated by subtracting the respective control value.

Bortezomib treatment studies. For in vivo treatment experiments, LICs of each leukemia model were injected into sublethally irradiated mice: 1 × 10^3 cells in the MLL-ENL or BCR-ABL/NUP98-HOXA9 models, and 1 × 10^4 cells in the MOZ-TIF2 model. Bortezomib was administrated i.p. at doses of 1.0 mg/kg twice weekly for 3 weeks. Treatment was started 1 week after transplantation in the MLL-ENL or BCR-ABL/NUP98-HOXA9 models, and 2 weeks after transplantation in the MOZ-TIF2 model. For experiments analyzing changes in LIC populations, bortezomib was administrated i.p. at doses of 1.0 mg/kg into fully developed leukemic mice. GFP^+ BM cells were collected 24 hours after injection, and surface marker profiles were analyzed.

Analysis of microarray data. We analyzed publicly available gene expression microarray data on murine and human samples from the Gene Expression Omnibus (GEO) database (GEO GSE24797, GSE20377, and GSE24006). A set of CEL files were downloaded from GEO and normalized using the JustRMA function from the Affy package 1.22.1 in Bioconductor. To compare expression profiles of the NF-κB target genes, normalized data were tested for GSEA using previously described NF-κB target gene sets (29), and a nominal *P* value was calculated. For screening of genes with elevated expression levels in LICs compared with those in normal HSPCs, the expression values of individual genes were compared between groups. Genes significantly elevated in LICs from all three leukemia models as determined by an unpaired Student's *t* test ($P < 0.05$)

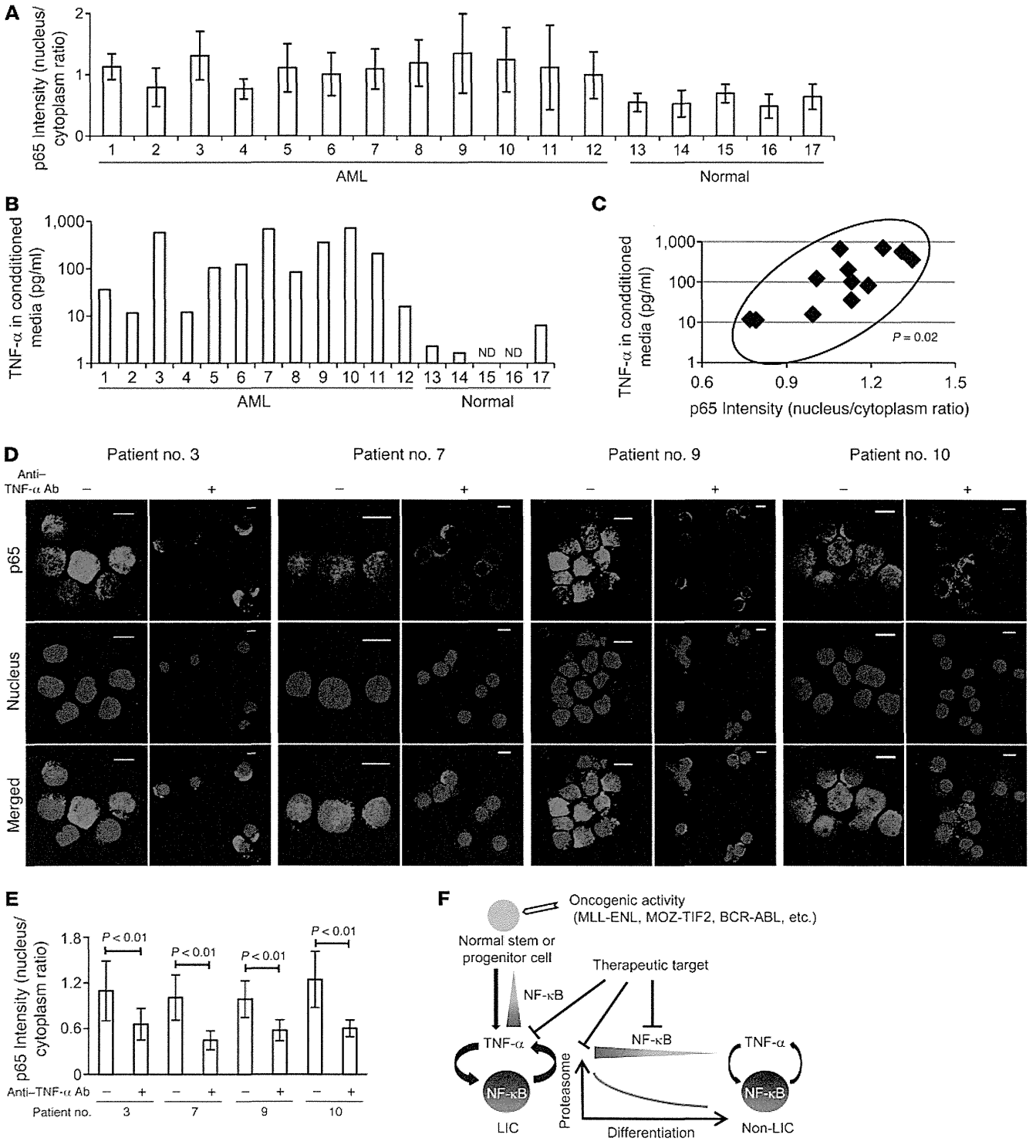

Figure 7

NF-κB/TNF-α positive feedback loop is activated in human AML LICs. (**A**) Quantification of p65 nuclear translocation assessed by the mean nucleus/cytoplasm intensity ratio by immunofluorescence staining. The $CD34^+CD38^-$ fractions isolated from AML or normal BM were analyzed. More than 50 cells were scored in each specimen, and the average intensity ratio with SD is shown. (**B**) TNF-α concentration of culture media conditioned by human AML LICs and normal HSCs measured by ELISA. ND, not detected. (**C**) Correlation between p65 nuclear translocation intensity ratio and TNF-α secretory ability of human AML LICs. (**D**) Immunofluorescence assessment of p65 nuclear translocation in LICs purified from 4 patients after serum-free culture with neutralizing antibody against TNF-α or isotype control. Scale bars: 10 μm. (**E**) Quantification of p65 nuclear translocation of LICs with or without neutralizing antibody against TNF-α assessed by the mean nucleus/cytoplasm intensity ratio. (**F**) Proposed model showing the role of NF-κB signaling in LICs. Positive feedback loop involving NF-κB/TNF-α promotes the maintenance and proliferation of LICs. The signaling is supported by active proteasome machinery, which declines with LIC differentiation.

were selected, among which genes also elevated in human AML LICs (Student's *t* test set at $P < 0.01$) were ultimately selected.

Statistics. Statistical significance of differences between groups was assessed with a 2-tailed unpaired Student's *t* test. Differences were considered statistically significant at a *P* value of less than 0.05. LIC frequency was calculated by Poisson statistics. In leukemia cell transplantation experiments, the overall survival of mice in BM transplantation assays is depicted by a Kaplan-Meier curve. Survival between groups was compared using the log-rank test. To measure the correlation between NF-κB intensity and TNF-α secretion in human AML samples, the Spearman's rank correlation coefficient was used.

Study approval. A total of 12 BM cells derived from patients with AML were obtained from the Department of Hematology and Oncology of the University of Tokyo Hospital. Five BM cells from patients diagnosed with lymphoid neoplasia without BM invasion were used as normal controls. The study was approved by the ethics committee of the University of Tokyo, and written informed consent was obtained from all patients whose samples were collected. All animal experiments were approved by the University of Tokyo Ethics Committee for Animal Experiments.

Acknowledgments

We thank T. Kitamura for the Plat-E packaging cells; H. Nakauchi and M. Onodera for the pGCDNsam-IRES-EGFP retroviral vector; R. Ono and T. Nosaka for the MLL-ENL cDNA; I. Kitabayashi for the MOZ-TIF2 cDNA; W. Hahn for the pBabe-GFP and pBabe-GFP-IκB-SR; and H. Algül and R.M. Schmid for providing the *Rela*-floxed mice. This work was supported by a Grant-in-Aid for Scientific Research A (KAKENHI 12020240) from the Ministry of Education, Culture, Sports, Science and Technology of Japan.

Received for publication December 3, 2012, and accepted in revised form October 17, 2013.

Address correspondence to: Mineo Kurokawa, Department of Hematology and Oncology, Graduate School of Medicine, The University of Tokyo, 7-3-1 Hongo, Bunkyo-ku, Tokyo 113-8655, Japan. Phone: 81.3.5800.9092; Fax: 81.3.5840.8667; E-mail: kurokawa-tky@umin.ac.jp.

1. Bonnet D, Dick JE. Human acute myeloid leukemia is organized as a hierarchy that originates from a primitive hematopoietic cell. *Nat Med.* 1997; 3(7):730–737.
2. Lapidot T, et al. A cell initiating human acute myeloid leukaemia after transplantation into SCID mice. *Nature.* 1994;367(6464):645–648.
3. Ishikawa F, et al. Chemotherapy-resistant human AML stem cells home to and engraft within the bone-marrow endosteal region. *Nat Biotechnol.* 2007; 25(11):1315–1321.
4. Marcucci G, Haferlach T, Döhner H. Molecular genetics of adult acute myeloid leukemia: prognostic and therapeutic implications. *J Clin Oncol.* 2011; 29(5):475–486.
5. Mardis ER, et al. Recurring mutations found by sequencing an acute myeloid leukemia genome. *N Engl J Med.* 2009;361(11):1058–1066.
6. Sen R, Baltimore D. Inducibility of kappa immunoglobulin enhancer-binding protein Nf-κB by a post-translational mechanism. *Cell.* 1986;47(6):921–928.
7. La Rosa FA, Pierce JW, Sonenshein GE. Differential regulation of the c-myc oncogene promoter by the NF-κB rel family of transcription factors. *Mol Cell Biol.* 1994;14(2):1039–1044.
8. Guttridge DC, Albanese C, Reuther JY, Pestell RG, Baldwin AS Jr. NF-κB controls cell growth and differentiation through transcriptional regulation of cyclin D1. *Mol Cell Biol.* 1999;19(8):5785–5799.
9. Duckett CS. Apoptosis and NF-κB: the FADD connection. *J Clin Invest.* 2002;109(5):579–580.
10. Karin M, Greten FR. NF-κB: linking inflammation and immunity to cancer development and progression. *Nat Rev Immunol.* 2005;5(10):749–759.
11. Karin M. Nuclear factor-κB in cancer development and progression. *Nature.* 2006;441(7092):431–436.
12. Pikarsky E, et al. NF-κB functions as a tumour promoter in inflammation-associated cancer. *Nature.* 2004;431(7007):461–466.
13. Guzman ML, et al. Nuclear factor-κB is constitutively activated in primitive human acute myelogenous leukemia cells. *Blood.* 2001;98(8):2301–2307.
14. Guzman ML, et al. Preferential induction of apoptosis for primary human leukemic stem cells. *Proc Natl Acad Sci U S A.* 2002;99(25):16220–16225.
15. Frelin C, et al. Targeting NF-κB activation via pharmacologic inhibition of IKK2-induced apoptosis of human acute myeloid leukemia cells. *Blood.* 2005;105(2):804–811.
16. Carvalho G, et al. Inhibition of NEMO, the regulatory subunit of the IKK complex, induces apoptosis in high-risk myelodysplastic syndrome and acute myeloid leukemia. *Oncogene.* 2007;26(16):2299–2307.
17. Guzman ML, et al. An orally bioavailable parthenolide analog selectively eradicates acute myelogenous leukemia stem and progenitor cells. *Blood.* 2007;110(13):4427–4435.
18. Jenkins C, et al. Nuclear factor-κB as a potential therapeutic target for the novel cytotoxic agent LC-1 in acute myeloid leukaemia. *Br J Haematol.* 2008;143(5):661–671.
19. Jin Y, et al. Antineoplastic mechanism of niclosamide in acute myelogenous leukemia stem cells: inactivation of the NF-κB pathway and generation of reactive oxygen species. *Cancer Res.* 2010;70(6):2516–2527.
20. Takahashi S, et al. Over-expression of Flt3 induces NF-κB pathway and increases the expression of IL-6. *Leuk Res.* 2005;29(8):893–899.
21. Liu S, et al. Sp1/NFκB/HDAC/miR-29b regulatory network in KIT-driven myeloid leukemia. *Cancer Cell.* 2010;17(4):333–347.
22. Nakagawa M, et al. AML1/RUNX1 functions as a cytoplasmic attenuator of NF-κB signaling in the repression of myeloid tumors. *Blood.* 2011; 118(25):6626–6637.
23. Eppert K, et al. Stem cell gene expression programs influence clinical outcome in human leukemia. *Nat Med.* 2011;17(9):1086–1093.
24. Sarry JE, et al. Human acute myelogenous leukemia stem cells are rare and heterogenous when assayed in NOD/SCID/IL2Rγc-deficient mice. *J Clin Invest.* 2011;121(1):384–395.
25. Liu T, et al. Functional characterization of meningioma 1 as collaborating oncogene in acute leukemia. *Leukemia.* 2010;24(3):601–612.
26. Kvinlaug BT, et al. Common and overlapping oncogenic pathways contribute to the evolution of acute myeloid leukemias. *Cancer Res.* 2011; 71(12):4117–4129.
27. Neering SJ, et al. Leukemia stem cells in a genetically defined murine model of blast-crisis CML. *Blood.* 2007;110(7):2578–2585.
28. Wang Y, et al. The Wnt/β-catenin pathway is required for the development ofleukemia stem cells in AML. *Science.* 2010;327(5973):1650–1653.
29. Hinz M, et al. Nuclear factor κB-dependent gene expression profiling of Hodgkin's disease tumor cells, pathogenetic significance, and link to constitutive signal transducer and activator of transcription 5a activity. *J Exp Med.* 2002;196(5):605–617.
30. Gentles AJ, Plevritis SK, Majeti R, Alizadeh AA. Association of a leukemic stem cell gene expression signature with clinical outcomes in acute myeloid leukemia. *JAMA.* 2010;304(24):2706–2715.
31. Kishore N, et al. A selective IKK-2 inhibitor blocks NF-κB-dependent gene expression in interleukin-1 β-stimulated synovial fibroblasts. *J Biol Chem.* 2003;278(35):32861–32871.
32. Algül H, et al. Pancreas-specific RelA/p65 truncation increases susceptibility of acini to inflammation-associated cell death following cerulein pancreatitis. *J Clin Invest.* 2007;117(6):1490–1501.
33. Beg AA, Finco TS, Nantermet PV, Baldwin AS Jr. Tumor necrosis factor and interleukin-1 lead to phosphorylation and loss of IκBα: a mechanism for NF-κB activation. *Mol Cell Biol.* 1993;13(6):3301–3310.
34. DeNardo DG, Coussens LM. Inflammation and breast cancer. Balancing immune response: crosstalk between adaptive and innate immune cells during breast cancer progression. *Breast Cancer Res.* 2007;9(4):212.
35. McLean MH, et al. The inflammatory microenvironment in colorectal neoplasia. *PLoS One.* 2011; 6(1):e15366.
36. Charles KA, et al. The tumor-promoting actions of TNF-α involve TNFR1 and IL-17 in ovarian cancer in mice and humans. *J Clin Invest.* 2009; 119(10):3011–3023.
37. Moore RJ, et al. Mice deficient in tumor necrosis factor-α are resistant to skin carcinogenesis. *Nat Med.* 1999;5(7):828–831.
38. Popivanova BK, et al. Blocking TNF-α in mice reduces colorectal carcinogenesis associated with chronic colitis. *J Clin Invest.* 2008;118(2):560–570.
39. Egberts JH, et al. Anti-tumor necrosis factor therapy inhibits pancreatic tumor growth and metastasis. *Cancer Res.* 2008;68(5):1443–1450.
40. Li J, et al. TNF-α induces leukemic clonal evolution ex vivo in Fanconi anemia group C murine stem cells. *J Clin Invest.* 2007;117(11):3283–3295.
41. Hoang T, Levy B, Ouetto N, Hainan A, Rodriguez-Cimadevilla JC. Tumor necrosis factor α stimulates the growth of the clonogenic cells of acute myeloblastic leukemia in synergy with granulocyte-macrophage colonystimulating factor. *J Exp Med.* 1989;170(1):15–26.
42. Khoury E, et al. Tumor necrosis factor alpha (TNF α) downregulates c-kit proto-oncogene product expression in normal and acute myeloid leukemia $CD34^+$ cells via p55 TNF alpha receptors. *Blood.* 1994;84(8):2506–2514.
43. Zhang B, et al. Altered microenvironmental regulation of leukemic and normal stem cells in chronic myelogenous leukemia. *Cancer Cell.* 2012; 21(4):577–592.
44. Kerbauy DM, Lesnikov V, Abbasi N, Seal S, Scott B, Deeg HJ. NF-κB and FLIP in arsenic trioxide (ATO)-induced apoptosis in myelodysplasticsyndromes (MDSs). *Blood.* 2005;106(12):3917–3925.
45. Adams J. The development of proteasome inhibitors as anticancer drugs. *Cancer Cell.* 2004;5(5):417–421.
46. Chen L, Madura K. Increased proteasome activity,

ubiquitin-conjugating enzymes, and eEF1A translation factor detected in breast cancer tissue. *Cancer Res.* 2005;65(13):5599–5606.
47. Stein SJ, Baldwin AS. Deletion of the NF-κB subunit p65/RelA in the hematopoietic compartment leads to defects in hematopoietic stem cell function. *Blood.* 2013;121(25):5015–5024.
48. Iversen PO, Wiig H. Tumor necrosis factor α and adiponectin in bone marrow interstitial fluid from patients with acute myeloidleukemia inhibit normal hematopoiesis. *Clin Cancer Res.* 2005; 11(19 pt 1):6793–6799.
49. Pronk CJ, Veiby OP, Bryder D, Jacobsen SE. Tumor necrosis factor restricts hematopoietic stem cell activity in mice: involvement of 2 distinct receptors. *J Exp Med.* 2011;208(8):1563–1570.
50. Taniguchi T, Takata M, Ikeda A, Momotani E, Sekikawa K. Failure of germinal center formation and impairment of response to endotoxin in tumor necrosis factor alpha-deficient mice. *Lab Invest.* 1997; 77(6):647–658.
51. Schmittgen TD, Livak KJ. Analyzing real-time PCR data by the Comparative C(T) method. *Nat Protoc.* 2008;3(6):1101–1108.
52. Jain AK, Bloom DA, Jaiswal AK. Nuclear import and export signals in control of Nrf2. *J Biol Chem.* 2005;280(32):29158–29168.

nature COMMUNICATIONS

ARTICLE

Received 29 Jan 2014 | Accepted 21 Jul 2014 | Published 27 Aug 2014

DOI: 10.1038/ncomms5770

Recurrent *CDC25C* mutations drive malignant transformation in FPD/AML

Akihide Yoshimi[1,*], Takashi Toya[1,*], Masahito Kawazu[2], Toshihide Ueno[3], Ayato Tsukamoto[1], Hiromitsu Iizuka[1], Masahiro Nakagawa[1], Yasuhito Nannya[1], Shunya Arai[1], Hironori Harada[4], Kensuke Usuki[5], Yasuhide Hayashi[6], Etsuro Ito[7], Keita Kirito[8], Hideaki Nakajima[9], Motoshi Ichikawa[1], Hiroyuki Mano[3] & Mineo Kurokawa[1]

Familial platelet disorder (FPD) with predisposition to acute myelogenous leukaemia (AML) is characterized by platelet defects with a propensity for the development of haematological malignancies. Its molecular pathogenesis is poorly understood, except for the role of germline *RUNX1* mutations. Here we show that *CDC25C* mutations are frequently found in FPD/AML patients (53%). Mutated CDC25C disrupts the G2/M checkpoint and promotes cell cycle progression even in the presence of DNA damage, suggesting a critical role for CDC25C in malignant transformation in FPD/AML. The predicted hierarchical architecture shows that *CDC25C* mutations define a founding pre-leukaemic clone, followed by stepwise acquisition of subclonal mutations that contribute to leukaemia progression. In three of seven individuals with *CDC25C* mutations, *GATA2* is the target of subsequent mutation. Thus, *CDC25C* is a novel gene target identified in haematological malignancies. *CDC25C* is also useful as a clinical biomarker that predicts progression of FPD/AML in the early stage.

[1] Department of Hematology and Oncology, Graduate School of Medicine, The University of Tokyo, 7-3-1 Hongo, Bunkyo-ku, Tokyo 113-8655, Japan. [2] Department of Medical Genomics, Graduate School of Medicine, The University of Tokyo, 7-3-1 Hongo, Bunkyo-ku, Tokyo 113-8655, Japan. [3] Department of Cellular Signaling, Graduate School of Medicine, The University of Tokyo, 7-3-1 Hongo, Bunkyo-ku, Tokyo 113-8655, Japan. [4] Department of Hematology, Juntendo University School of Medicine, 3-1-3 Hongo, Bunkyo-ku, Tokyo 113-8431, Japan. [5] Department of Hematology, NTT Medical Center Tokyo, 5-9-22 Higashi-Gotanda, Shinagawa-ku, Tokyo 141-8625, Japan. [6] Department of Hematology/Oncology, Gunma Children's Medical Center, 779 Simohakoda, Kitaakebonocho, Shibukawa-shi, Gunma 377-8577, Japan. [7] Department of Pediatrics, Graduate School of Medicine, Hirosaki University, 53 Honmachi, Hirosaki-shi, Aomori 036-8563, Japan. [8] Department of Hematology and Oncology, University of Yamanashi, 1110 Simokawakita, Chuou-shi, Yamanashi 409-3898, Japan. [9] Division of Hematology, Department of Internal Medicine, Keio University School of Medicine, 35 Shinanomachi, Shinjyuku-ku, Tokyo 160-8582, Japan. * These authors contributed equally to this work. Correspondence and requests for materials should be addressed to M.K. (email: kurokawa-tky@umin.ac.jp).

Familial platelet disorder (FPD)/acute myelogenous leukaemia (AML) (MIM601399) is an autosomal dominant disorder with inherited thrombocytopenia, abnormal platelet function and a lifelong risk of the development of a variety of haematological malignancies[1], such as AML, myelodysplastic syndromes (MDS) and myeloproliferative neoplasms. Although inherited *RUNX1* mutations are the cause of the congenital thrombocytopenia, it remains unclear whether a mutation in *RUNX1*, which is generally known to have a dominant-negative effect[2–4], is sufficient to induce the development of haematological malignancies in individuals with FPD/AML. It is also not known whether additional gene mutations are required for the transformation, and, if so, which genes are involved. Given that only 40% of FPD/AML patients develop these neoplasms[5] and that a relatively long period is required for subsequent *RUNX1* mutation-mediated development of neoplasms in FPD/AML, the secondary genetic events may function as a driver to promote malignant transformation. We reasoned that identifying gene mutations responsible for the malignant transformation of FPD/AML would provide indispensable information for addressing these questions. However, only about 30 pedigrees with FPD/AML have been reported so far, and the rarity of this disorder has impeded the establishment of clinical diagnostic criteria and the clinical improvement to refine cancer therapy and to identify biomarkers that would allow detection of patients at risk for the onset of malignancies in FPD/AML.

We collected DNA samples and clinical information of 73 individuals, belonging to 57 pedigrees, who have a history of familial thrombocytopenia and/or haematological malignancies, with the aim of identifying pedigrees with FPD/AML and uncovering recurrent mutations that drive the malignant transformation. Next-generation sequencing and single-cell sequencing strategy suggest that somatic mutation in *CDC25C* may be one of the early genetic events for leukaemic initiation in FPD/AML, and further stepwise acquisition of mutations such as *GATA2* leads to FPD/AML-associated leukaemic progression. These observations shed light on a part of leukemogenesis in FPD/AML.

Results

A novel gene target in haematological disorders. Thirteen patients in 7 pedigrees were diagnosed as having FPD/AML after screening for germline *RUNX1* mutations in 73 index patients; 7 of the 13 patients had developed haematological malignancies, while the other 6 only showed thrombocytopenia (Table 1). Most of the detected *RUNX1* mutations were point mutation in Runt homology domain or frame-shift mutation that lost transactivation domain, consistent with the previous reports[2,4]. As haploinsufficiency of *RUNX1* might cause familial thrombocytopenia with propensity to develop AML[1], we also examined whether the pedigrees have *RUNX1* loss of heterozygosity (LOH) or not. A synchronized quantitative-PCR method[6] and single-nucleotide polymorphism (SNP) sequencing detected no case with LOH in *RUNX1* in our cohort (Supplementary Fig. 1 and detailed in Methods). To systematically identify additional genetic alterations, we utilized whole-exome sequencing for two individuals from the same FPD/AML pedigree who shared a common *RUNX1*_p.Phe303fs mutation and who had developed MDS (subject 20) or myelofibrosis (subject 21) at the age of 37 and 17 years, respectively. In both these patients, the disease had progressed to AML[7]. Validation by Sanger sequencing and/or targeted deep sequencing of candidate mutations in paired tumour/normal DNA samples confirmed 10 (subject 20) and 8 (subject 21) somatically acquired nonsynonymous mutations (Table 2; Supplementary Figs 2–4; Supplementary Methods). Surprisingly, both patients carried the identical somatic *CDC25C* mutation (p.Asp234Gly), which had not been reported previously in human cancers (Fig. 1a,b). Prompted by this finding, we investigated *CDC25C* mutations in other FPD/AML cases by deep sequencing. In total, four of seven affected patients with haematological malignancies had *CDC25C* mutations, of which three carried the same p.Asp234Gly mutation. Moreover, *CDC25C* mutations were detected in an additional three FPD/AML patients who had not yet developed haematological malignancies, although the variant allele fractions (VAFs) were much lower in this group of patients than in those who had already developed haematological malignancies (Fig. 1c; Table 1). Thus, 7 of the 13 FPD/AML patients (53%) harboured a *CDC25C* mutation. *CDC25C* was also screened for mutations in 90 sporadic MDS and 53 AML patients, including 13 MDS and 3 AML cases who carried *RUNX1* mutations. No *CDC25C* mutations were identified in the 90 sporadic cases, except for the p.Ala344Val in an MDS patient bearing a *RUNX1* mutation, indicating that *CDC25C* mutations were significantly associated with germline, but not with somatic *RUNX1* mutations ($P = 0.004$; Supplementary Fig. 5; Supplementary Table 1).

Clonal evolution of FPD/AML. Deep sequencing of individual mutations that had been detected by whole-exome sequencing

Table 1 | Mutational status of *CDC25C* in FPD/AML patients.

Pedigree number	Subject number	RUNX1 mutation	Disease status	Age, years*	CDC25C mutation	VAF (%)
18	20	p.Phe303fs	MDS/AML	37/38	p.Asp234Gly	31.7/45.8
	21		MF/AML	17/18	p.Asp234Gly	31.1/39.0
19	22	p.Arg174*	AML	41	p.His437Asn	39.7
54	65	p.Ser140Asn	MDS	25	—	—
	66		AML	56	p.Asp234Gly	24.2
32	38	p.Leu445Pro	HCL	72	—	—
16	18	p.Thr233fs	Thrombocytopenia	—	p.Asp234Gly	5.9
53	62	p.Gly262fs	MDS	12	—	—
	63		Thrombocytopenia	—	—	—
	67		Thrombocytopenia	—	—	—
57	71	p.Gly172Glu	Pancytopenia†	—	p.Asp234Gly	8.3
	72		Thrombocytopenia	—	—	—
	73		Thrombocytopenia	—	p.Lys233Glu	1.8

AML, acute myeloid leukemia; FPD, familial platelet disorder; HCL, hairy cell leukemia; MDS, myelodysplastic syndrome; MF, myelofibrosis; VAF, variant allele fraction.
*Age at the time of diagnosis of each haematological malignancy is shown.
†Thrombocytopenia, leukopenia and iron-deficiency anemia were diagnosed.

Table 2 | Validated somatic mutations.

Gene symbol	Ref seq_no.	Amino-acid change	Position (hg19)	Base change	Mutation type	SIFT prediction	VAF at MDS/MF (%)	VAF at AML (%)
Subject 20								
AGAP4	NM_133446	p.Arg484Cys	g.chr10:46321905	C->T	Missense	Damaging	13.2	11.5
CDC25C	NM_001790	p.Asp234Gly	g.chr5:137627720	A->G	Missense	Damaging	31.7	45.8
CHEK2	NM_007194	p.Arg406His	g.chr22:29091740	G->A	Missense	Tolerated	14.6	11.1
COL9A1	NM_001851	p.Gly878Val	g.chr6:70926733	G->T	Missense	Damaging	9.6	26.4
DTX2	NM_001102594	p.Pro74Arg	g.chr7:76110047	C->G	Missense	Damaging	18.3	11.2
FAM22G	NM_001170741	p.Ser508Thr	g.chr9:99700727	T->A	Missense	Tolerated	10.2	27.6
GATA2	NM_001145661	p.Leu321His	g.chr3:128202758	T->A	Missense	Damaging	0.0	28.1
LPP	NM_001167671	p.Val538Met	g.chr3:188590453	G->A	Missense	Damaging	9.7	28.8
RP1L1	NM_178857	p.Ser215fs	g.chr8:10480295	insC	Frameshift	Damaging	14.2	12.7
SIGLEC9	NM_014441	p.Ser437Gly	g.chr19:51633253	A->G	Missense	Tolerated	27.4	42.5
Subject 21								
ANXA8L1	NM_001098845	p.Val281Ala	g.chr10:48268018	T->C	Missense	Damaging	30.8	36.8
CDC25C	NM_001790	p.Asp234Gly	g.chr5:137627720	A->G	Missense	Damaging	31.1	39.1
DENND5A	NM_001243254	p.Arg320Ser	g.chr11:9215218	A->C	Missense	Damaging	29.5	37.3
FER	NM_005246	p.Tyr634Cys	g.chr5:108382876	A->G	Missense	Damaging	1.4	30.4
FNDC1	NM_032532	p.Arg189Cys	g.chr6:159636081	C->T	Missense	Damaging	29.3	35.9
OR8U1	NM_001005204	p.Asn175Ile	g.chr11:56143623	A->T	Missense	Damaging	30.0	34.1
PIDD	NM_145886	p.Arg342Cys	g.chr11:802347	C->T	Missense	Damaging	3.3	28.3
ZNF614	NM_025040	p.Glu202Gly	g.chr19:52520246	A->G	Missense	Damaging	28.7	33.7

AML, acute myeloid leukemia; MDS, myelodysplastic syndrome; MF, myelofibrosis; SIFT, sorting intolerant from tolerant; VAF, variant allele fraction.

allowed accurate determination of their VAFs; on this basis, we could establish an inferred model of clonal evolution in terms of individual mutations in subjects 20 and 21 (Fig. 2a,b; Supplementary Fig. 6a,b). Intratumoral heterogeneity was evident at both MDS and AML phases in subject 20. According to the predicted model, a founding clone with a *CDC25C* mutation acquired additional mutations in *COL9A1*, *FAM22G* and *LPP* (group A), followed by the emergence of a *GATA2* mutation (group B), which was associated with leukaemic transformation, whereas the size of another subclone, defined by mutations in *CHEK2* and three other genes (group C), was unchanged. To validate this hierarchical model, single-cell genomic sequencing was performed using genomic DNA of 63 bone marrow cells from subject 20 when the patient was in the AML phase. Assuming that all cells harbour the *RUNX1* mutation, the false-negative rate of the procedure reached 35%, possibly due to biased allele amplification (Online Methods). However, this technique successfully demonstrated that the group A/B and group C mutations were mutually exclusive (Fig. 2c; Supplementary Table 2). To statistically evaluate this possibility, we assumed two hypotheses (H_0: the mutational status of genes in group A/B and group C is independent; H_1: mutations in group A/B and group C are mutually exclusive) and calculated each probability distribution (P_i: probability that the current results as shown in Fig. 2c were obtained under the hypothesis H_i). Our mutational profile data were achieved with a much higher likelihood under H_1 than H_0 (Supplementary Fig. 7 and detailed in Supplementary Methods). Similarly, the clonal architecture for subject 21 was portrayed in Fig. 2b and Supplementary Fig. 6b. In both scenarios, *CDC25C* mutations seemed to represent a founding mutation with the highest VAF, suggesting that the *CDC25C* mutation contributed to the establishment of a founding tumour population as an early genetic event, whereas progression to AML seemed to be accompanied by the appearance of additional mutations, indicating a multistep process in leukemogenesis.

Along with the somatic mutations found in subjects 20 and 21, a *GATA2* mutation was also identified in subject 22 (Fig. 3a). This patient developed AML with multilineage dysplasia, which led to the diagnosis of AML – MRC (myelodysplasia-related changes). Remission-induction therapies were only partially effective and the blast cell count was reduced from 54 to 5.6%, while dysplastic features persisted (Fig. 3b; Supplementary Fig. 8). Allogeneic stem cell transplantation was successfully performed from a human leukocyte antigen-matched unrelated donor and durable complete remission, with 100% donor chimerism, was achieved. During treatment, the VAF of the *GATA2* mutation decreased virtually in parallel with the blast cell percentage, while the VAF of the *CDC25C* mutation hovered at a high level before transplantation. Thus, we hypothesized that the *GATA2* mutation induced leukaemia progression in this patient, whereas the *CDC25C* mutation was associated with the pre-leukaemic status. Another *GATA2* mutation (p.Leu359Val) was found in subject 18, with a VAF (0.94%), who showed only thrombocytopenia without any signs of leukaemia progression and who had a small subclone with a concurrent *CDC25C* mutation (Fig. 3c). Although *GATA2* mutations are detected in a small number of patients with FPD/AML, the findings described above suggest that mutation of *GATA2* is a key factor promoting disease progression in FPD/AML (Fig. 3d).

Biological consequences of *CDC25C* mutations. We next investigated the possible impact of *CDC25C* mutation on clonal selection and evolution. CDC25C is a phosphatase that prevents premature mitosis in response to DNA damage at the G2/M checkpoint, while it is constitutively phosphorylated at Ser216 throughout interphase by c-TAK1 (refs 8–10). When phosphorylated at Ser216, CDC25C binds to 14-3-3 protein[11], leading to sequestration of CDC25C to the cytoplasm and its inactivation. Ba/F3 cells were transduced with retroviruses encoding the wild-type or mutant CDC25C containing each of the individual mutations (p.Asp234Gly, p.Ala344Val, p.His437Asn and p.Ser216Ala), and assayed for the phosphorylation status, 14-3-3 protein-binding capacity and intracellular localization of each of these proteins. The Ser216Ala mutant form

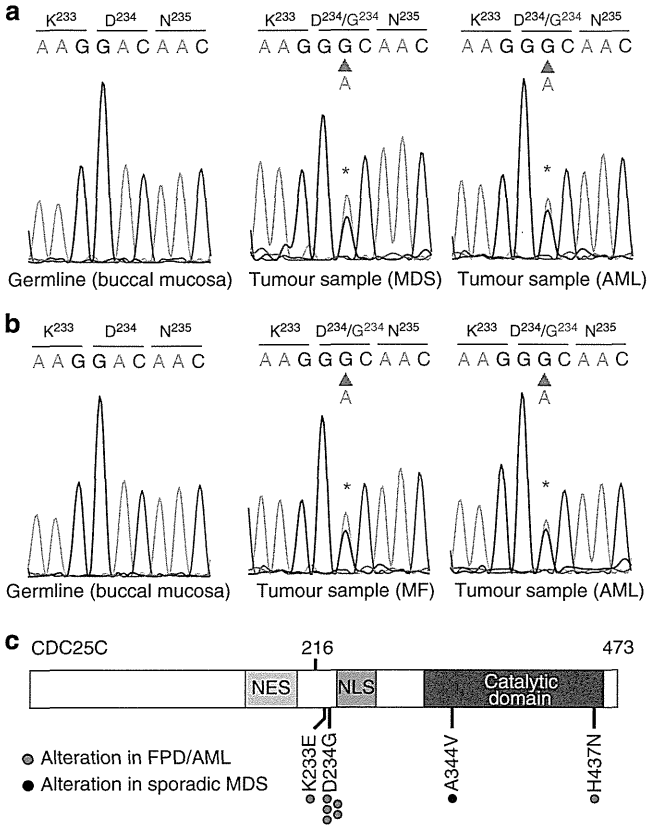

Figure 1 | Mutation in *CDC25C* recurs in cases of FPD/AML. (**a**,**b**) Sanger sequencing of *CDC25C* mutations found in whole-exome sequencing is shown. Both forward and reverse traces were available for each mutation, but only one trace is shown above. The results of buccal mucosa, pre-leukaemic phase and leukaemic phase is demonstrated for subject 20 (**a**) and subject 21 (**b**), respectively. (**c**) The distribution of alterations is shown for the CDC25C protein. NES, a putative nuclear export signal domain between amino acids 177–200; NLS, a putative nuclear localization sequence domain consisting of amino acids 240–244.

of CDC25C, which lacks the phosphorylation site, was used as a negative control. In all of the mutated forms of CDC25C, the capacity for binding to c-TAK1 was reduced (Fig. 4a,b; Supplementary Fig. 9a,b), resulting in decreased phosphorylation of CDC25C at Ser216 (Fig. 4c). Consequently, the mutant proteins failed to bind 14-3-3 protein efficiently (Fig. 4d,e; Supplementary Fig. 8c,d) and remained in the nucleus even during interphase (Fig. 4f; Supplementary Figs 10 and 11). In accordance with these observations, CDC25C mutants enhanced mitotic entry, which was exaggerated by low-dose radiation-induced DNA damage (Fig. 4g,h; Supplementary Fig. 12; Supplementary Methods). These results suggest that mutation of *CDC25C* results in disruption of the DNA checkpoint machinery. Next, we investigated why mutation of *CDC25C* is a frequent genetic event in FPD/AML. It is known that *RUNX1* mutations suppress DNA damage repair and subsequent cell cycle arrest in hematopoietic cells by means of transcriptional suppression of several genes that are involved in DNA repair[12,13]. We confirmed that FPD/AML-associated *RUNX1* mutations have similar effects, as we observed activation of the G2/M checkpoint mechanism in the presence of *RUNX1* mutations (Fig. 4i; Supplementary Fig. 13a,b). We found, however, that introduction of mutations in *CDC25C* resulted in enhanced mitosis entry, despite co-existence of *RUNX1* mutations (Fig. 4i). Therefore, we speculated that compromised DNA damage checkpoint mechanisms caused by mutations in *CDC25C* may contribute to malignant transformation, in concert with increased genomic instability due to *RUNX1* mutations.

Discussion

Whole-exome sequencing, followed by targeted deep sequencing, identified novel aspects of the pathogenesis of malignant transformation in FPD/AML. First, the high frequency of *CDC25C* mutations in FPD/AML underscores their major role in the development of haematological malignancies in FPD/AML patients. To our knowledge, *CDC25C* mutations have not been reported previously and represent a new recurrent mutational target in haematological malignancies, although *CDC25C* mutations have been reported in some solid carcinomas with unknown significance[14,15]. Furthermore, our functional assays support their biological significance, which is characterized by cell cycle progression and premature mitotic entry. Although the 5q31 minimally deleted region, in which CDC25C is located, is frequently detected in MDS, it seems to be associated with other oncogenic mechanisms since our functional assays suggested that *CDC25C* mutations in FPD/AML were gain-of-function type mutations that facilitate the mitotic entry by aberrant accumulation in the nucleus. Impaired DNA repair function mediated by germline *RUNX1* mutation may play a role in the generation of *CDC25C* mutations.

Evaluation of the allelic burden of mutated genes demonstrated that *CDC25* mutations are found with high VAFs in FPD/AML-derived leukaemia and with low VAFs in cases of thrombocytopenia. Our hierarchical model and clonal selection highlighted that mutation of *CDC25C* defines an initial event during malignant transformation and predates subclonal mutations in *GATA2* and other genes. On the basis of the observation that four of the seven FPD/AML patients with *CDC25C* mutations have developed leukaemia and that *CDC25C* mutations were actually detected in the leukaemic subclones, we speculated that a FPD/AML patient with a *CDC25C* mutation, but without clinically evident leukaemia, is at high risk for the onset of leukaemic progression. Examination of the allelic burden of *CDC25C* mutation may thus serve to evaluate the risk of leukaemic progression in patients with FPD/AML.

Among the mutations found in FPD/AML, mutations in *GATA2* were identified in 3 of 13 individuals (subjects 18, 20 and 22). *GATA2* mutations were frequently identified in FPD/AML-derived leukaemia (2/7) and in a patient with thrombocytopenia who had a small subclone bearing a *CDC25C* mutation (1/6). Although reports on the clinical relevance of *GATA2* mutations in myeloid malignancy are limited, several lines of evidence in this respect have recently been reported. *GATA2* mutations are frequently found in a subgroup of patients with cytogenetically normal AML with biallelic *CEBPA* gene mutations[16], which account for ~4% of AML. Germline *GATA2* mutations are also observed in disorders linked to an increased propensity for the development of MDS and AML, including Emberger syndrome, MonoMAC syndrome and dendritic cells, monocytes, B and natural killer cells deficiency[17–20]. The alterations in *GATA2* (leading to p.Leu321His and p.Leu359Val), which were found in FPD/AML patients in this study, are located in the part of the gene encoding the N-terminal and C-terminal zinc-finger domains, respectively (Fig. 3d). Mutations affecting the identical amino acids have been reported in AML patients bearing *CEBPA* mutations and chronic myeloid leukaemia patients in blast crisis[16,21]. Thus, *GATA2* mutation may contribute to AML progression in collaboration with *RUNX1* and/or *CDC25C* mutations. Furthermore, although

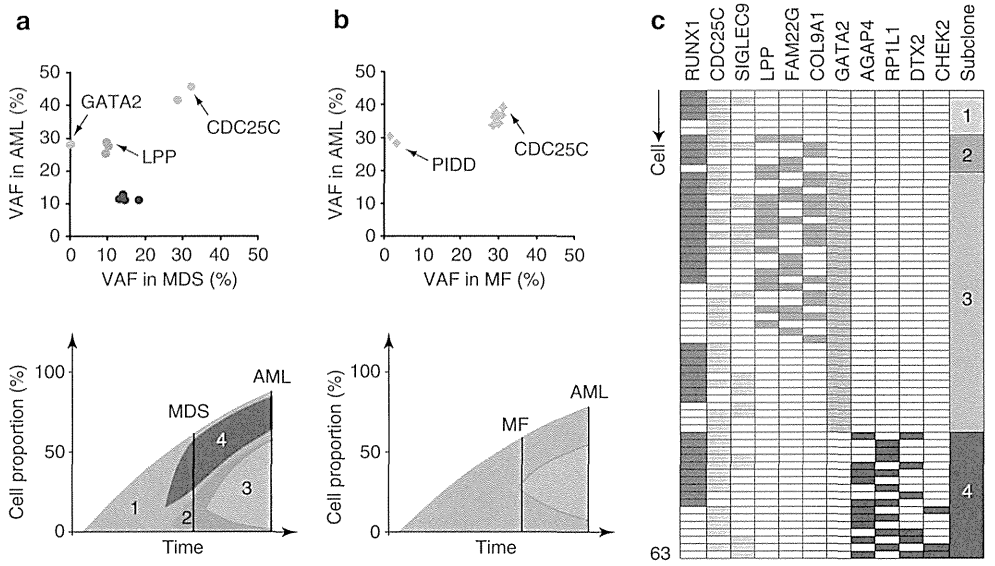

Figure 2 | Clonal evolution of FPD/AML-related myeloid disorders. (**a**,**b**) Observed variant allele fraction (VAF) of validated mutations are listed in Table 2, in both pre-leukaemic and leukaemic phases, are shown in diagonal plots (top) for subject 20 (**a**) and subject 21 (**b**). Predicted chronological behaviours in different leukemia subclones are depicted below each diagonal plot. Distinct mutation clusters are displayed by colour. The vertical axis represents cell proportion of each clone calculated by VAF × 2 (%) (because all the mutations were heterozygous), regarding the whole bone marrow as 100%. (**c**) Mutation status of each bone marrow cell from subject 20 during the acute myeloid leukemia (AML) phase. The vertical axis represents each cell ($n = 63$) and the horizontal axis displays each gene mutation. Coloured columns show that the corresponding cell harbours gene mutation(s) as defined in Online Methods. Subclone numbers shown in the right row correspond to the numbers in the lower figure of **a**.

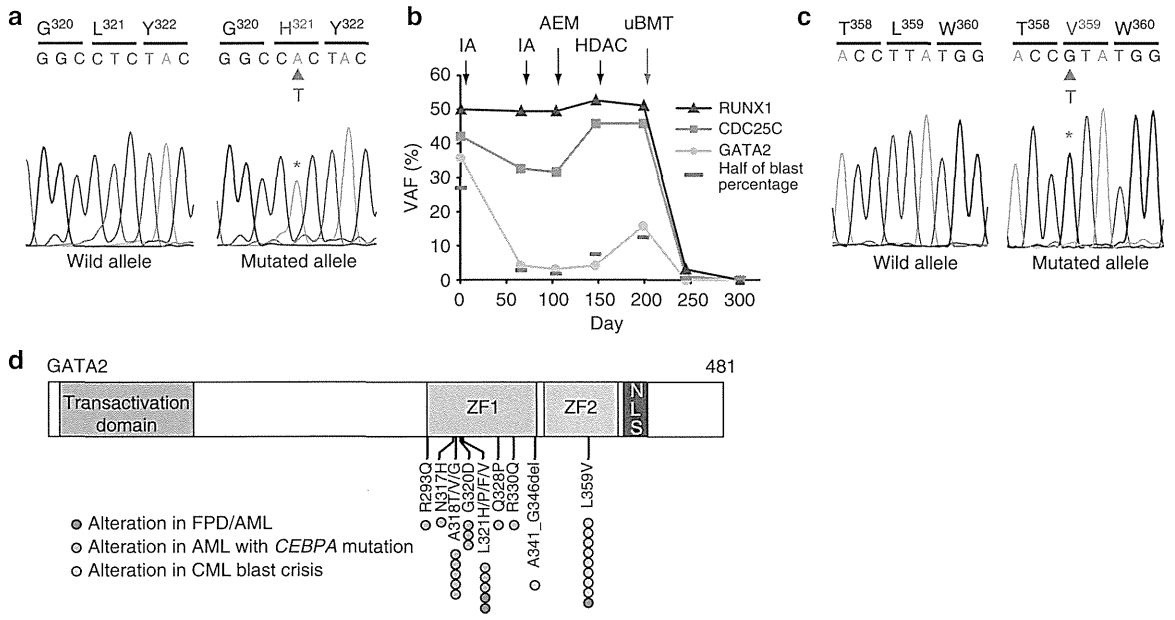

Figure 3 | *GATA2* mutations in FPD/AML. The result of Sanger sequencing for *GATA2* p.Leu321His mutation in subject 22 (**a**) and Leu359Val mutation in subject 18 (**c**) validated with subcloning strategy by methods shown in Supplementary Methods. (**b**) Variant allele fractions (VAFs) of *RUNX1*, *CDC25C* and *GATA2* mutation in subject 22 are demonstrated with the time course of treatment. Half the value of the blast cell percentage, which corresponds to the allele frequency of a heterozygous mutation, is also shown by a red bar. IA, idarubicine + Ara-C; AEM, Ara-C + etoposide + mitoxantrone; HDAC, high-dose Ara-C; uBMT, unrelated bone marrow transplantation. (**d**) Schematic representation of *GATA2* mutations. *GATA2* mutations that were identified in FPD/AML are displayed together with mutations found in AML with *CEBPA* mutation[16] as well as in CML patients in blast crisis[21]. ZF, zinc-finger domain; NLS, a putative nuclear localization sequence domain.

another report identified somatic *CBL* mutation with acquired 11q uniparental disomy as a second hit as being responsible for leukaemic transformation in FPD/AML[22], *CBL* mutations were not detected in our series of FPD/AML samples.

Although the precise pathogenetic roles of *CDC25C* mutations remain unclear, we presume that mutant CDC25C alleles confer a proliferative advantage under certain circumstances in which DNA repair machinery is compromised, such as that mediated by

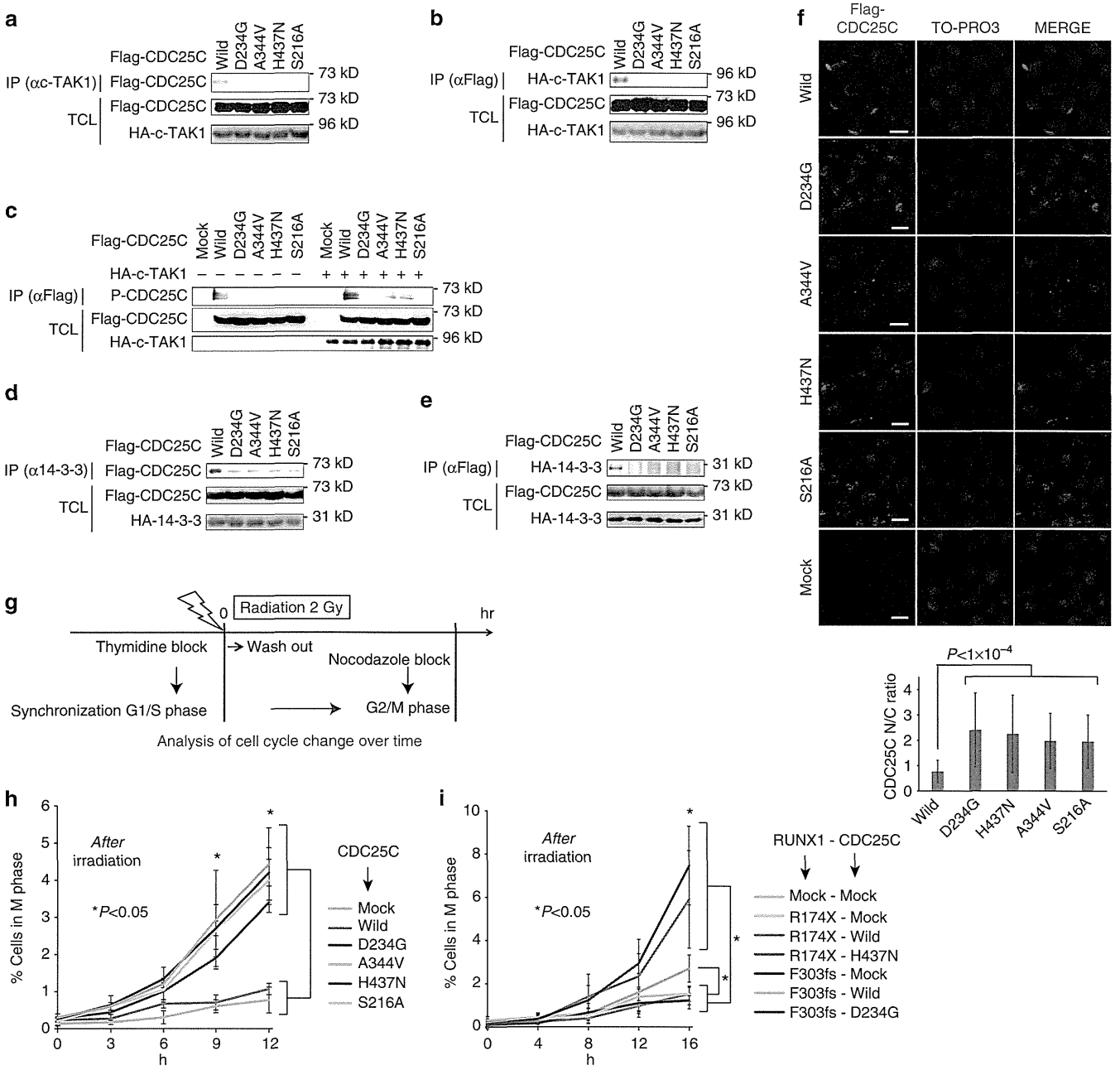

Figure 4 | Mutated CDC25C enhances mitotic entry. (**a**) HEK293T cells were transiently transfected with constructs encoding Flag-tagged CDC25C wild type or mutants, as indicated, and cell lysates were immunoprecipitated with anti-c-TAK1 antibody. Binding capacity of CDC25C was evaluated by western blotting. IP, immunoprecipitation; TCL, total cell lysate. (**b**) Reciprocal immunoprecipitation of **a** using anti-Flag (CDC25C) antibody for immunoprecipitation. (**c**) Left half; cell lysates were immunoprecipitated with anti-Flag antibody. Phosphorylation levels of CDC25C were assessed by phosphorylated-Ser216-specific anti-CDC25C antibody. Right half; the same experiment was performed with cell lysates from HEK293T cells transfected with constructs encoding Flag-tagged CDC25C wild type or mutants and HA-tagged c-TAK1. (**d**) Mutated CDC25C showed reduced capacity for binding to 14-3-3. Cell lysates were immunoprecipitated with anti-14-3-3 antibody and binding capacity of CDC25C was evaluated. (**e**) Reciprocal immunoprecipitation of **d** using anti-Flag (CDC25C) antibody for immunoprecipitation. (**f**) Localization of CDC25C or its mutants was visualized by immunofluorescence. Anti-Flag antibody and Alexa Fluor 555 antibody was used for visualization of CDC25C. N/C ratio of each cell was calculated as detailed in Supplementary Methods and Supplementary Fig. 10. The mean and s.d. of the N/C ratio is presented. Statistical significance of difference was determined by unpaired Student's *t*-test ($n>30$ for each). Scale bar, 10 μm. (**g**) Schematic description of the method used for evaluation of mitotic entry. (**h**) Mitotic entry of CDC25C-mutated cells. Percentage of mutated CDC25C-transduced cells in the M phase was compared with that of wild-type CDC25C-transduced cells. *P* values were calculated using Student's *t*-test and the differences between groups, as indicated, were all statistically significant ($^*P<0.05$) at 10 and 12 h after irradiation ($n=3$). The average and s.d. is presented. (**i**) Mutated RUNX1 and CDC25C were co-expressed in Ba/F3 cells, as indicated, and mitosis entry of these cells was evaluated. The differences between groups, as indicated, were all statistically significant ($^*P<0.05$ at 16 h after washout of thymidine ($n=3$). *P* values were determined using the Student's *t*-test. The average and s.d. is presented.

a germline *RUNX1* mutation. In addition, as Turowski and colleagues reported that CDC25C was involved in S phase entry in addition to mitotic entry[23], release from thymidine-induced G1/S block may be affected by some unknown machinery mediated by mutated CDC25Cs, which might affect the results when we observed G2/M phase fraction of these cells. It is not clear why *CDC25C* mutations are repetitively documented in FPD/AML, but not in sporadic MDS or AML cases. One possibility is that in the presence of a *RUNX1* mutation, as an initial event, an extended period is required before an additional *CDC25C* mutation is acquired. This proposal is supported by the clinical observation that ~40% of patients with FPD/AML develop leukaemia in their 30s[5]; however, the mutational status in *CDC25C* in the reported cohort was unknown.

One of the important problems in the research of FPD/AML is that definitive diagnostic criteria have not been established yet. For this purpose, more extensive studies are required for accumulating clinical characterization, genetic information and functional examination as to whether a *RUNX1* variant in families with thrombocytopenia and/or haematological malignancy is causal[24]. We clarified tentative diagnostic criteria for FPD/AML, which was used in this study (in Methods). Regarding the three missense variants in our study (p.Ser140Asn in pedigree 54, p.Gly172Glu in pedigree 57 and p.Leu445Pro in pedigree 32), Ser140 and Gly172 have been reported to be mutated in sporadic AML and/or MDS cases[25,26]. In addition, induced pluripotent stem cells from a FPD/AML pedigree with p.Gly172Glu recapitulate the phenotype of FPD/AML after hematopoietic differentiation[27]. Ser140 has been also shown to be important for RUNX1 conformation, and a mutation of this site affects hydrogen bonds and results in functional loss[28,29]. Furthermore, all the three missense variants have not been reported in the following SNP database: SNP database (dbSNP) (http://www.ncbi.nlm.nih.gov/projects/SNP), the 1000 Genomes Project (http://www.1000genomes.org), HGVB (http://www.genome.med.kyoto-u.ac.jp/SnpDB/index.html). They were also predicted as 'damaging' by Polyphen-2 (http://genetics.bwh.harvard.edu/pph2/), SIFT (http://sift.jcvi.org/) and PROVEAN (http://provean.jcvi.org/index.php). Therefore, we regarded the pedigrees with these *RUNX1* variants as having FPD/AML in this study. However, regarding pedigree 32 with p.Leu445Pro, we could not completely exclude the possibility of incidental co-occurrence of a possible non-causal *RUNX1* germline variant and hairy cell leukaemia, although co-occurrence of them is supposed to be rare. In addition, we should bear in mind the somatic as well as germline LOH of *RUNX1*, which contributes to thrombocytopenia and/or leukemogenesis in FPD/AML.

In conclusion, our results indicate that FPD/AML-associated leukaemic transformation is due to stepwise acquisition of mutations and clonal selection, which is initiated by a *CDC25C* mutation in the pre-leukaemic phase, and is further driven by mutations in other genes including *GATA2* (Supplementary Fig. 14). The identification of *CDC25C* as the target gene responsible for the leukaemic transformation will facilitate diagnosis and monitoring of individuals with FPD/AML, who are at an increased risk of developing life-threatening haematological malignancy.

Methods

Subjects. Studies involving human subjects were done in accordance with the ethical guidelines for biomedical research involving human subjects, which was developed by the Ministry of Health, Labour and Welfare, Japan; the Ministry of Education, Culture, Sports, Science, and Technology, Japan; and the Ministry of Economy, Trade, and Industry, Japan, and enforced on 29 March 2001. This study was approved by ethical committee of the University of Tokyo and each participating institution. Written informed consent was obtained from all patients whose samples were collected after the guideline was enforced. All animal experiments were approved by the University of Tokyo Ethics Committee for Animal Experiments. The clinical data, peripheral blood sample and buccal mucosa of the patients whose pedigree contained two or more individuals with thrombocytopenia and/or any haematological malignancies were collected from participating institutions. Platelet threshold depended on each institution's judge and any haematological malignancies were allowed. The diagnoses were self-reported. When all the following four criteria were fulfilled, the patient was considered as having FPD/AML in this study: (1) the pedigree has two or more individuals with thrombocytopenia and/or any haematological malignancies; (2) a germline *RUNX1* variant, including missense, nonsense, frameshift, insertion and deletion, is confirmed by Sanger sequencing and a synchronized quantitative-PCR method in at least one family member; (3) the *RUNX1* variant has not been reported in public dbSNP; (4) no germline mutations were detected in the following 16 genes: *GATA2, GATA1, CEBPA, MPL, MYH9, MYL9, GP1BA, GP9, MASTL, HOXA11, CBL, DIDO1, TERT, ANKRD26, GFI1B* and *SRP72*. Regarding the last criterion, 16 genes were selected because they have been reported to be responsible for familial thrombocytopenia and/or haematological malignancies.

Whole-exome sequencing. Genomic DNA was extracted from samples using the QIAamp DNA Mini kit (Qiagen). Exome capture was performed. Enriched exome fragments were subjected to sequencing using HiSeq2000 (Illumina). We removed any potential somatic mutations that were observed in dbSNP (http://www.ncbi.nlm.nih.gov/projects/SNP) or in the 1000 Genomes Project (http://www.1000genomes.org) data. All candidate single-nucleotide variations and indels, which were predicted to be deleterious by the Polyphen-2 algorithm, were validated by deep sequencing and Sanger sequencing. Genomic DNA samples from the buccal mucosa of the two patients (subject 20 and subject 21) were used as references. All candidate somatic mutations were validated by Sanger sequence and deep sequencing using primers listed in Supplementary Tables 3 and 4.

Deep sequencing. Using genomic DNA of the patients as template, each targeted region was PCR amplified with specific primers (Supplementary Table 4). The amplification products from an individual sample were combined and purified with the AMpure XP Kit (Beckman Coulter) and library preparation was carried out using the Ion Xpress Fragment Library Kit (Life Technologies) according to the manufacturer's instructions. The Agilent 2100 Bioanalyzer (Agilent Technologies) and the associated High Sensitivity DNA kit (Agilent Technologies) were used to determine quality and concentration of the libraries. The amount of the library required for template preparation was calculated using the template dilution factor calculation described in the protocol. Emulsion PCR and enrichment steps were carried out using the Ion OneTouch 200 Template Kit v2 DL (Life Technologies). Sequencing was undertaken using Ion Torrent PGM and Ion 318 chips Kit v2 (Life Technologies). The Ion PGM 200 Sequencing Kit (Life Technologies) was used for sequencing reactions, following the recommended protocol. The presence of *CDC25C* and *GATA2* mutations was also validated by a subclone strategy for DNA sequence analysis.

Single-cell sequencing and genome amplification. Single cells were separated from the bone marrow of subject 20 at AML phase using FACSAria II (BD biosciences) (Supplementary Fig. 15a). Each cell was deposited into individual wells of a 96-well plate. Single cells were lysed and whole genome from single cell was amplified using GenomePlex Single Cell Whole-Genome Amplification Kit (Sigma-Aldrich). Mutation status of each gene was analysed by direct sequencing with specific primers (Supplementary Table 5). To improve the sensitivity of this procedure, we used multiple primer sets for detecting a single-nucleotide variation. We estimated the false-negative rate of this procedure based on the ratio of RUNX1 mutation, which is supposed to be observed in all of the cells. The false-negative rate was estimated to be 35% (22 cells out of 63 cells, Supplementary Table 2), which is consistent with the manufacturer's bulletin reporting the allelic dropout of 30%. In light of these results, we regard those cells with at least one gene mutation in a mutational group (coloured in red, orange, green, blue or purple) as being positive for gene mutations of the corresponding group. To assess whether mutations in *LPP, FAM22G, COL9A1* and *GATA2* and mutations in *AGAP4, RP1L1, DTX2* and *CHEK2* were mutually exclusive, we performed a statistical analysis as follows. First of all, we determine a matrix **A** that virtually represents the mutational status of eight genes (1: *LPP*, 2: *FAM22G*, 3: *COL9A1*, 4: *GATA2*, 5: *AGAP4*, 6: *RP1L1*, 7: *DTX2* and 8: *CHEK2*) of 57 cells. Concretely, **A** is defined as follows:

$$\mathbf{A}=\begin{pmatrix} a_{1,1} & \cdots & a_{8,1} \\ \vdots & \ddots & \vdots \\ a_{1,57} & \cdots & a_{8,57} \end{pmatrix} \quad a_{i,j}=\begin{cases} 0 : \text{if gene i of cell j is wildtype} \\ 1 : \textit{if} \text{ gene i of cell j is mutated} \end{cases} \qquad (1)$$

On the other hand, a matrix **R** indicates data from the actual experimental results of mutational analysis as shown in Fig. 2c. Elements of **R** is provided in

Supplementary Table 2.

$$\mathbf{R}=\begin{pmatrix} r_{1,1} & \cdots & r_{8,1} \\ \vdots & \ddots & \vdots \\ r_{1,57} & \cdots & r_{8,57} \end{pmatrix} \quad r_{i,j}=\begin{cases} 0 : \text{if gene i of cell j is wild type} \\ 1 : \text{if gene i of cell j is mutated} \\ 2 : \text{if mutational status of gene i of cell j is undetermined} \end{cases} \tag{2}$$

Then we assumed two hypotheses: H_0 and H_1.

H_0: the mutational status of genes $1\sim4$ and genes $5\sim8$ is independent. Each matrix elements of **A** are randomly assigned 0 or 1 (at ratio of 1:1) independently of each other.

H_1: mutations in genes $1\sim4$ and genes $5\sim8$ are mutually exclusive, and cells $1\sim40$ harbour mutations of genes $1\sim4$, while cells $41\sim57$ harbour mutations of genes $5\sim8$. In mathematical representation,

$$a_{i,j}=\begin{cases} 0 : (5\le i\le 8 \text{ and } 1\le j\le 40) \text{ and } (1\le i\le 4 \text{ and } 41\le j\le 57) \\ 0 \text{ or } 1 \text{ randomely} : (1\le i\le 4 \text{ and } 1\le j\le 40) \text{ and } (5\le i\le 8 \text{ and } 41\le j\le 57) \end{cases} \tag{3}$$

We assumed matrices $\mathbf{A}_0$ and $\mathbf{A}_1$ that represent virtually generated mutational status under the hypotheses H_0 and H_1, and calculate the probability of substantializing **R** for given $\mathbf{A}_0$ and $\mathbf{A}_1$.

$P_0(\mathbf{R}/\mathbf{A}_0)$ and $P_1(\mathbf{R}/\mathbf{A}_1)$ can be calculated for given matrices $\mathbf{A}_0$ and $\mathbf{A}_1$ under the condition as follows:

Probability that we cannot determine whether a cell has mutation in gene X when the cell does not actually have a mutation; 28% (based on our data shown in Supplementary Table 2).

Probability that we judge that a cell has a mutation in gene X when the cell does not actually have a mutation; 5% (because it is very unlikely to happen).

Probability that we can judge correctly that a cell does not have a mutation in gene X when the cell does not actually have a mutation; 67% ($100-28-5=67\%$).

Probability that we cannot determine whether a cell has mutation in gene X when the cell actually has a mutation; 28% (based on our data shown in Supplementary Table 2).

Probability that we judge that a cell has a mutation in gene X when the cell actually has a mutation; 35% (the estimated false-negative rate based on the ratio of *RUNX1* mutation).

Probability that we can judge correctly that a cell has a mutation in gene X when the cell actually has a mutation; 37% ($100-28-35=37\%$).

Put it simply, $\mathbf{P}_0$ represents the probability that one can get the mutational profile R when a cell harbours mutations independently of each other, while $\mathbf{P}_1$ indicates the probability that R is realized under the condition where mutations in gene groups $1\sim4$ and $5\sim8$ are exclusive. Because $\mathbf{A}_0$ and $\mathbf{A}_1$ that meet the hypotheses H_0 and H_1 can be generated innumerably, we conducted a computational simulation to acquire the distribution of P_0 and P_1 by generating $\mathbf{A}_0$ and $\mathbf{A}_1$ 100,000 times. For visibility, horizontal axis is converted to $-\ln(P)$.

Synchronized quantitative-PCR. These experiments were performed mostly as described previously[6]. Briefly, genomic DNA was denatured 95 °C for 5 min and iced immediately. Using the LightCycler 480 Instrument II (Roche), thermal cycling was performed with denatured genomic DNA, forward and reverse primers (Supplementary Table 6), THUNDERBIRD SYBR qPCR mix (TOYOBO). Threshold cycle scores were determined as the average of triplicate samples. We designed 27 primers for *RUNX1* and 3 reproducible primers (that is, primer RUNX-9, RUNX-19 and RUNX-20) were chosen by preparatory experiments. RPL5-2 and PRS7-1 primers, which were authorized previously[6], were also utilized as controls. In addition, genomic DNA extracted from the bone marrow sample of a MDS patient with a chromosome 21 deletion was also examined with the same primers as a control of *RUNX1* locus copy-number loss. Crossing points (Cps) of designed primers were examined by quantitative PCR. *RUNX1* locus copy-number relative to RPL5-2 was calculated using Cps of RUNX-9 and RPL5-2, with RPL5-2 values set at 2. Similar results were obtained when Cps of RUNX-19, RUNX-20 or RPS7-1 values were used.

LOH detection with SNP sequencing. To examine the existence of uniparental disomy, we designed four specific primers to detect nine SNPs in *RUNX1*, which are frequently seen (>40%) (Supplementary Table 7). Direct sequencing was performed with the primers, and heterogeneity of SNPs was examined.

Chemicals and immunological reagents. Thymidine and nocodazole were purchased from Sigma-Aldrich. Anti-CDC25C, anti-phospho-CDC25C (Ser216) and anti-beta-actin antibodies were purchased from Cell Signaling Technology. Anti-HA monoclonal antibody was purchased from MBL. Rabbit anti-Flag monoclonal antibody was purchased from Sigma-Aldrich. Anti-HA was purchased from Roche. Mouse anti-phospho-histone H2AX (Ser139) antibody and Alexa Fluor 488 mouse anti-phospho-H3 (Ser10) antibody were purchased from Merck Millipore. Alexa Fluor 488 rabbit anti-mouse immunoglobulin (Ig)G, Alexa Fluor 488 goat anti-rabbit IgG and Alexa Fluor 555 goat anti-rabbit IgG were purchased from Invitrogen. TO-PRO3 was purchased from Molecular Probes. Rabbit anti-14-3-3 Sigma antibody was purchased from Bethyl laboratories. Sheep anti-c-TAK1 antibody was purchased from Exalpha Biologicals. Anti-sheep IgG-HRP was purchased from RSD. Nonviable cell exclusion was performed by 7-AAD Viability Staining Solution (BioLegend).

Subclone strategy and direct sequencing. Using genomic DNA of the patients as template, each targeted region was amplified by PCR with specific primers (Supplementary Table 4). PCR products were purified with illustra ExoStar (GE Healthcare) and subcloned into *Eco*RV site of pBluescript II KS(−) (Stratagene). Ligated plasmids were transformed into *E. coli* strain XL1-Blue by 45 s heat shock at 42 °C. Positive transformants were incubated on LB plates containing 100 μg ml^{-1} ampicillin supplemented with X-gal (Sigma-Aldrich) and isopropyl β-D-1-thiogalactopyranoside (Sigma-Aldrich). For colony PCR, a portion of a white colony was directly added to a PCR mixture as the DNA template. Insert region was amplified by PCR procedure with T3 and T7 universal primers, purified with illustra ExoStar (GE Healthcare Life Sciences), and sequenced by the Sanger method with T3 and T7 primers using BigDye Terminator v3.1 Cycle Sequencing kit (Applied Biosystems) and ABI Prism 310 Genetic Analyzer (Life Technologies).

Immunoprecipitation and western blotting. These experiments were performed as described previously[30]. Briefly, HEK293T cells were transiently transfected with mammalian expression plasmids encoding Flag-tagged CDC25C and its mutants, HA-tagged 14-3-3 or c-TAK1. All plasmids were sequence verified. After 48 h, cell lysates were collected and incubated with an antibody (anti-HA antibody (1:200, 3 h), anti-Flag antibody (1:200, 3 h), anti-c-TAK1 antibody (1:150, 3 h) and anti 14-3-3 antibody (1:150, 3 h)). After incubation, the cell lysates were incubated with protein G-Sepharose (GE Healthcare) for 1 h. The precipitates were stringently washed with high salt-containing wash buffer and analysed by western blotting. Anti-Flag (HRP-conjugated, Sigma-Aldrich), anti-HA (MBL), anti-HA (HRP-conjugated, Roche), anti-CDC25C (Cell Signaling Technology), anti-phospho-CDC25C (Ser216) (Cell Signaling Technology), anti-c-TAK1 antibody (Exalpha Biologicals) or anti-14-3-3 antibody (Bethyl laboratories) antibodies and Immunostar LD (Wako) was used for detection. Original gel images of western blot analysis are shown in Supplementary Fig. 16.

Cell cycle synchronization and analysis for mitosis entry. After transduction of wild-type CDC25C or its mutated forms to murine lymphoid cell line Ba/F3 cells (RIKEN BioResource Center), double-thymidine block was performed to obtain cell cycle synchronization at G1/S phase. In brief, 2 mM of thymidine was added to the medium. After 16 h, cells were washed and released from the first thymidine for 8 h. A second block was initiated by adding 2 mM of thymidine, and cells were maintained for 16 h. Then thymidine was washed out and the cells were incubated with 1 mM nocodazole with or without 2 Gy of irradiation (Supplementary Fig. 10a). Ba/F3 cells were fixed over time with 75% ethanol in phosphate-buffered saline (PBS) at 4 °C overnight and permeabilized with 2% Triton-X at 4 °C for 15 min. The cells were stained with anti-phospho-H3 (Ser10) Alexa Fluor 488 conjugated antibody (dilution, 1:200) in PBS with 2% fetal calf serum at 4 °C for 30 min and then treated with 5% propidium iodide and 1% RNase in PBS at room temperature (RT) for 30 min. Cell cycle was analysed using a BD LSR II Flow cytometer (BD biosciences) (Supplementary Fig. 15b). To assess the cooperation of *CDC25C* and *RUNX1* mutation, wild-type or mutant (D234G, H437N) pMXs-neo-Flag-CDC25C and mutant (F303fsX566, R174X) pGCDNsam-IRES-KusabiraOrange-Flag-RUNX1 were retrovirally transduced into Ba/F3 cells.

Immunofluorescent microscopic analysis. These experiments were performed as described previously[30]. Briefly, Ba/F3 cells were fixed, permeabilized and blocked. Staining for phosphorylated histone H2AX was performed with anti-phospho-histone H2AX (Ser139) antibody (dilution, 1:500; Merck Millipore) at RT for 3 h. After washing with PBS three times and with 1% bovine serum albumin in PBS, the cells were treated with Alexa Fluor 488 rabbit anti-mouse IgG (dilution, 1:500; Invitrogen) and TO-PRO3 (dilution, 1:1,000; Molecular Probes) for 1 h. The proteins were visualized using FV10i (Olympus) or BZ-9000 (Keyence). The percentage of γH2AX foci-positive cells was determined by examining 100 cells per sample. Three independent experiments were performed. To evaluate the localization of CDC25C, Ba/F3 cells were treated with 2 mM thymidine for 12 h and stained. Staining was underwent with anti-Flag antibody or anti-CDC25C antibody at RT for 3 h. After washing, the cells were treated with Alexa Fluor 488 or 555 antibody and TO-PRO3 for 1 h. The mean intensity of CDC25C in the nucleus and cytoplasm of each cell was measured within a region of interest placed within the nucleus and cytoplasm (Supplementary Fig. 10). Similarly, the background intensity was quantified within the region of interest placed outside the cells. All the measurements were performed using the Fluoview FV10i software or ImageJ. The background-subtracted intensity ratio of the nucleus to cytoplasm was calculated in >30 cells in each specimen.

Retrovirus production. The procedures were performed as described previously[30]. Briefly, Plat-E packaging cells were transiently transfected with each retroviral construct using the calcium phosphate precipitation method, and supernatant

containing retrovirus was collected 48 h after transfection and used for infection after it was centrifuged overnight at 10,000 r.p.m.

Statistical analysis. To compare data between groups, unpaired Student's *t*-test was used when equal variance were met by the *F*-test. When unequal variances were detected, the Welch *t*-test was used. Differences were considered statistically significant at a *P* value of <0.05.

References

1. Song, W. J. *et al.* Haploinsufficiency of CBFA2 causes familial thrombocytopenia with propensity to develop acute myelogenous leukaemia. *Nat. Genet.* **23,** 166–175 (1999).
2. Ichikawa, M. *et al.* A role for RUNX1 in hematopoiesis and myeloid leukemia. *Int. J. Hematol.* **97,** 726–734 (2013).
3. Cameron, E. R. & Neil, J. C. The Runx genes: lineage-specific oncogenes and tumor suppressors. *Oncogene* **23,** 4308–4314 (2004).
4. Nickels, E. M., Soodalter, J., Churpek, J. E. & Godley, L. A. Recognizing familial myeloid leukemia in adults. *Ther. Adv. Hematol.* **4,** 254–269 (2013).
5. Liew, E. & Owen, C. Familial myelodysplastic syndromes: a review of the literature. *Haematologica* **96,** 1536–1542 (2011).
6. Kuramitsu, M. *et al.* Extensive gene deletions in Japanese patients with diamond-blackfan anemia. *Blood* **119,** 2376–2384 (2012).
7. Kirito, K. *et al.* A novel RUNX1 mutation in familial platelet disorder with propensity to develop myeloid malignancies. *Haematologica* **93,** 155–156 (2008).
8. Boutros, R., Lobjois, V. & Ducommun, B. CDC25 phosphatases in cancer cells: key players? Good targets? *Nat. Rev. Cancer* **7,** 495–507 (2007).
9. Kastan, M. B. & Bartek, J. Cell-cycle checkpoints and cancer. *Nature* **432,** 316–323 (2004).
10. Peng, C. Y. *et al.* C-TAK1 protein kinase phosphorylates human Cdc25C on serine 216 and promotes 14-3-3 protein binding. *Cell Growth Differ.* **9,** 197–208 (1998).
11. Lopez-girona, A., Furnari, B., Mondesert, O. & Early, P. R. Nuclear localization of Cdc25 is regulated by DNA damage and a 14-3-3 protein. *Nature* **397,** 172–175 (1999).
12. Satoh, Y., Matsumura, I., Tanaka, H. & Harada, H. C-terminal mutation of RUNX1 attenuates the DNA-damage repair response in hematopoietic stem cells. *Leukemia* **26,** 303–311 (2011).
13. Krejci, O. *et al.* p53 signaling in response to increased DNA damage sensitizes AML1-ETO cells to stress-induced death. *Blood* **111,** 2190–2199 (2008).
14. Park, J. *et al.* Mutation profiling of mismatch repair-deficient colorectal cancers using an in silico genome scan to identify coding microsatellites advances in brief mutation profiling of mismatch repair-deficient colorectal cancers using an in silico genome scan to Ide. *Cancer Res.* **62,** 1284–1288 (2002).
15. Vassileva, V., Millar, A., Briollais, L., Chapman, W. & Bapat, B. Genes involved in DNA repair are mutational targets in endometrial cancers with microsatellite instability. *Cancer Res.* **62,** 4095–4099 (2002).
16. Greif, P. A. *et al.* GATA2 zinc finger 1 mutations associated with biallelic CEBPA mutations define a unique genetic entity of acute myeloid leukemia. *Blood* **120,** 395–403 (2012).
17. Ostergaard, P. *et al.* Mutations in GATA2 cause primary lymphedema associated with a predisposition to acute myeloid leukemia (Emberger syndrome). *Nat. Genet.* **43,** 929–931 (2011).
18. Hahn, C. N. *et al.* Heritable GATA2 mutations associated with familial myelodysplastic syndrome and acute myeloid leukemia. *Nat Genet.* **43,** 1012–1017 (2011).
19. Hsu, A. P. *et al.* Mutations in GATA2 are associated with the autosomal dominant and sporadic monocytopenia and mycobacterial infection (MonoMAC) syndrome. *Blood* **118,** 2653–2655 (2011).
20. Dickinson, R. E. *et al.* Exome sequencing identifies GATA-2 mutation as the cause of dendritic cell, monocyte, B and NK lymphoid deficiency. *Blood* **118,** 2656–2658 (2011).
21. Zhang, S.-J. *et al.* Gain-of-function mutation of GATA-2 in acute myeloid transformation of chronic myeloid leukemia. *Proc. Natl Acad. Sci. USA* **105,** 2076–2081 (2008).
22. Hasegawa, D. *et al.* CBL mutation in chronic myelomonocytic leukemia secondary to familial platelet disorder with propensity to develop acute myeloid leukemia (FPD/AML). *Blood* **119,** 2612–2614 (2012).
23. Turowski, P. *et al.* Functional cdc25C dual-specificity phosphatase is required for S-phase entry in human cells. *Mol. Biol. Cell* **14,** 2984–2998 (2003).
24. Michaud, J. *et al.* In vitro analyses of known and novel RUNX1/AML1 mutations in dominant familial platelet disorder with predisposition to acute myelogenous leukemia: Implications for mechanisms of pathogenesis. *Blood* **99,** 1364–1372 (2002).
25. Kohlmann, A. *et al.* Monitoring of residual disease by next-generation deep-sequencing of RUNX1 mutations can identify acute myeloid leukemia patients with resistant disease. *Leukemia* **28,** 129–137 (2014).
26. Chen, C. Y. *et al.* RUNX1 gene mutation in primary myelodysplastic syndrome - The mutation can be detected early at diagnosis or acquired during disease progression and is associated with poor outcome. *Br. J. Haematol.* **139,** 405–414 (2007).
27. Sakurai, M. *et al.* Impaired hematopoietic differentiation of RUNX1-mutated induced pluripotent stem cells derived from FPD/AML patients. *Leukemia.* (epub ahead of print 15 April 2014; doi:10.1038/leu.2014.136).
28. Bravo, J., Li, Z., Speck, N. A. & Warren, A. J. The leukemia-associated AML1 (Runx1)-CBF beta complex functions as a DNA-induced molecular clamp. *Nat. Struct. Biol.* **8,** 371–378 (2001).
29. Akamatsu, Y., Tsukumo, S. I., Kagoshima, H., Tsurushita, N. & Shigesada, K. A simple screening for mutant DNA binding proteins: application to murine transcription factor PEBP2?? subunit, a founding member of the Runt domain protein family. *Gene* **185,** 111–117 (1997).
30. Yoshimi, A. *et al.* Evi1 represses PTEN expression and activates PI3K/AKT/mTOR via interactions with polycomb proteins. *Blood* **117,** 3617–3628 (2011).

Acknowledgements

This work was supported in part by grants-in-aid from the Ministry of Health, Labor and Welfare of Japan (H23-Nanchi-Ippan-104; M. Kurokawa) and KAKENHI (24659457; M. Kurokawa). We thank R. Lewis (University of Nebraska Medical Center) and T. Kitamura (Institute of Medical Science, The University of Tokyo) for providing essential materials; T. Koike (Nagaoka Red Cross Hospital), K. Nara (Ootemachi Hospital), K. Suzuki (Japanese Red Cross Medical Center), H. Harada (Fujigaoka Hospital), Y. Morita (Kinki University), M. Matsuda (PL Hospital), H. Kashiwagi (Osaka University), T. Kiguchi (Chugoku Central Hospital), T. Masunari (Chugoku Central Hospital), K. Yamamoto (Yokohama City Minato Red Cross Hospital), T. Takahashi (Mitsui Memorial Hospital) and T. Takaku (Juntendo University) for providing patient samples; M. Kuramitsu (National Institutte of Infectious Diseases) for providing kind support of synchronized quantitative PCR; and K. Tanaka and Y. Shimamura for their technical assistance.

Author contributions

A.Y., T.T., M.I. and M. Kurokawa analysed genetic materials and performed functional studies. A.T., H.I., M.N., Y.N. and S.A. were involved in sequencing and/or functional studies. M. Kawazu, T.U. and H.M. took part in whole-exome sequencing, deep sequencing and bioinformatics analyses of the data. A.Y., T.T., M.I., H.H., K.U., Y.H., E.I., K.K. and H.N. collected specimens. A.Y. and T.T. generated figures and tables. M. Kurokawa designed and led the entire project. A.Y., T.T. and M. Kurokawa wrote the manuscript. All authors participated in the discussion and interpretation of the data.

Additional information

Accession codes: Sequence data for FPD/AML patients has been deposited in GenBank/EMBL/DDBJ sequence read archive (SRA) under the accession code SRP043031

Supplementary Information accompanies this paper at http://www.nature.com/naturecommunications

Competing financial interests: The authors declare no competing financial interests.

Reprints and permission information is available online at http://npg.nature.com/reprintsandpermissions

How to cite this article: Yoshimi, A. *et al.* Recurrent *CDC25C* mutations drive malignant transformation in FPD/AML. *Nat. Commun.* 5:4770 doi: 10.1038/ncomms5770 (2014).

12 腫瘍

2．組織球症

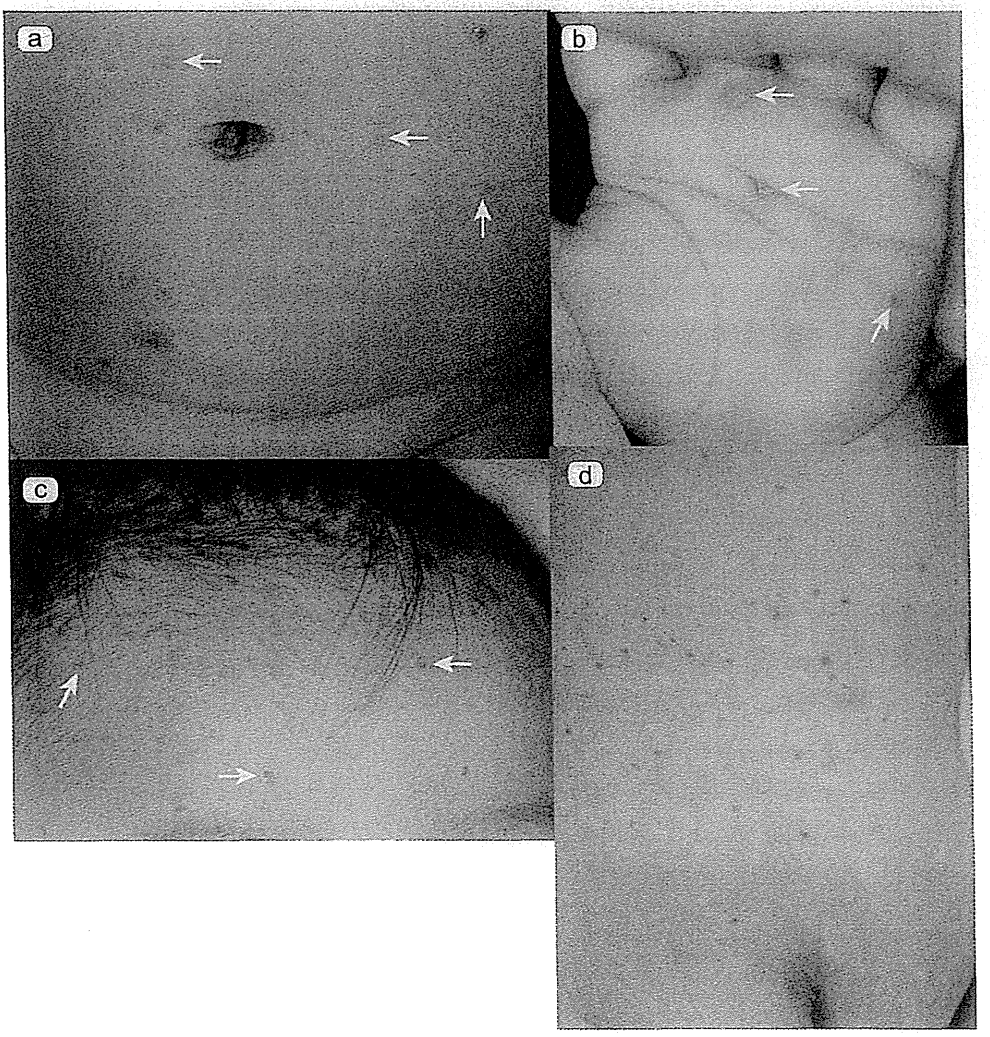

図1 ランゲルハンス細胞組織球症（LCH）の女児の臨床像

生後3週間より体幹，前額，手掌等に水疱出現。生後約3カ月時に当科（大阪大学皮膚科）受診（a～d）。ステロイド外用にても軽快せず，前額部の水疱はむしろ悪化（c）。体幹部は一部白斑も混じる（d）。生後約4カ月より両耳下腺部のリンパ節腫脹，脾腫出現。5カ月より熱発，貧血出現したためビンブラスチン・プレドニゾロンにて加療。1歳6カ月で骨髄移植。以後経過良好である。

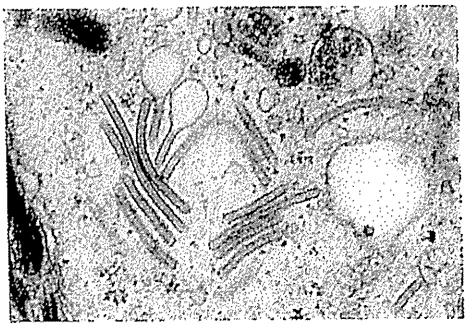

図2　LCH の男児皮膚より生検した組織の電子顕微鏡像
胞体内にラケット状の Birbeck 顆粒を認める。

1．組織球症とは

ランゲルハンス細胞などの樹状細胞やマクロファージがモノクローナルに増殖する疾患。皮膚，骨(頭蓋骨，長管骨等)，リンパ節，肺，肝，脾などの造血系，口腔粘膜，胃腸粘膜，胸腺，甲状腺，膵臓，腎臓，下垂体，眼窩，中枢神経系などさまざまな臓器に浸潤する。以下のように分類[1]。

① ランゲルハンス細胞組織球症 (Langerhans cell histiocytosis：LCH)
　Ⅰ：LCH-SS：単系統 (好酸球性肉芽腫症：多巣性骨病変)
　Ⅱ：LCH-MS：多系統で重要臓器(-)(Hand-Schüller-Christian 病：2～5 歳で発症し骨病変，眼球突出，尿崩症を 3 徴候)
　Ⅲ：LCH-MS(RO)：多系統で重要臓器 (肝，肺，脾，骨髄) を含む (Letterer-Siwe 病：2 歳未満で発症し多臓器に及ぶ)
② non-LCH：マクロファージの増殖による (若年性黄色腫，Rosai Dorfman 病，Erdheim-Chester 病)
③ 悪性組織球症

2．診断のポイント (以下 LCH について述べる)

初発症状は皮膚が多い。丘疹，水疱，びらん，結節，紫斑，ときに白斑など多彩な皮疹がさまざまな部位に出現するが図1，非特異的な症状であるため早期診断が困難である[2]。皮膚生検で診断する。免疫学的染色にて CD1a(+)，CD207(langerin)(+)。電子顕微鏡にて胞体内にラケット状の Birbeck 顆粒を認める図2。

3．検査

超音波検査 (肝脾腫，リンパ節腫大)，血液検査 (貧血，血小板減少，バソプレシン濃度低下)，X-P (頭蓋骨，長管骨)，MRI，骨髄穿刺，呼吸機能[3]。

4．治療

限局性の皮膚病変に対しては局所ステロイド外用を行う。LCH-MS 例に限り以前はビンブラスチン・プレドニゾロンが用いられていたが，最近では LCH の原因遺伝子の一つは *BRAF* と考えられており，これに対して海外で vemurafenib (2014 年 12 月現在国内未承認) 等による治療も試みられている[4]。骨髄移植が行われることもある[5]。

(村上有香子)

Pediatr Blood Cancer 2014;61:1215–1221

Improved Treatment Results of Children With B-Cell Non-Hodgkin Lymphoma: A Report From the Japanese Pediatric Leukemia/Lymphoma Study Group B-NHL03 Study

Masahito Tsurusawa, MD,[1]* Tetsuya Mori, MD,[2] Akira Kikuchi, MD,[3] Tetsuo Mitsui, MD,[4] Shosuke Sunami, MD,[5] Ryoji Kobayashi, MD,[6] Tetsuya Takimoto, MD,[7] Akiko Saito, MD, PhD,[8] Tomoyuki Watanabe, PhD,[9] Junichiro Fujimoto, MD,[7] Atsuko Nakazawa, MD,[10] Kouichi Ohshima, MD,[11] and Keizo Horibe, MD,[8] for the lymphoma committee of the Japanese Pediatric Leukemia/Lymphoma Study Group

Background. Previous Japanese studies of childhood B-cell non-Hodgkin lymphoma (B-NHL) have shown a favorable outcome, though the study size was too small to effectively assess the efficacy and safety of treatment for childhood B-NHL. ***Procedure.*** We performed a nation-wide prospective B-NHL03 study to assess the efficacy and safety of short-pulse intensive chemotherapy for children with B-NHL. They were stratified into four treatment groups according to disease stage, tumor resectability and bone marrow/CNS involvement: Group 1 with all resected stage I/II, Group 2 with non-resected stage I/II, Group 3 with stage III & CNS-negative stage IV, and Group 4 with CNS-positive stage IV & Burkitt leukemia. Treatment duration was 2 courses for Group 1, 4 courses for Group 2, and 6 courses for Groups 3 and 4, respectively. CNS irradiation was omitted in all patients. ***Results.*** The follow-up time ranged from 0.8 to 88 months, with a median of being 45 months. For 321 patients analyzed in this study, overall survival and event-free survival (EFS) at 4 years was 92.7% and 87.4%, respectively. The 4-year EFS according to treatment group were 94% for Group 1 (n = 17), 98% for Group 2 (n = 103), 84% for Group 3 (n = 111), and 78% for Group 4 (n = 90). There was no significant difference in outcome by histology. Therapy-related death occurred in three patients in remission. ***Conclusions.*** Our nationwide large-scale study resulted in a cure rate above 90% with <1% toxic death in childhood B-NHL. Pediatr Blood Cancer 2014;61:1215–1221.

Key words: B-NHL03; childhood; JPLSG; non-Hodgkin lymphoma

INTRODUCTION

Childhood B-cell non-Hodgkin Lymphoma (B-NHL) consists mainly of two histological subtypes, namely Burkitt lymphoma (BL), which includes Burkitt leukemia (B-ALL), and diffuse large B-cell lymphoma (DLBCL). The cure rate of childhood BL has been markedly improved over the past 30 years, and long-term event-free survival (EFS) of patients has reached to approximately 90%. This is largely due to prospective studies of European and North American groups that developed a short intensive chemotherapy regimen, including a high-dose methotrexate (HDMTX), an intermediate dose of cyclophosphamide (CPA), and anthracyclines [1–6]. Although DLBCL is a distinct disease entity from BL, the treatment is the same as that for patients with Burkitt histology, and excellent outcome has been reported [1–6]. Previously most clinical experiences of childhood B-NHL were reported by European and North American study groups, and there were few data on Japanese or Asian patients with B-NHL. In the1990s, we conducted group-wide trials for childhood B-NHL [7–10]: Horibe et al. showed a 4-year EFS with 70% for 57 patients (BL 31, B-ALL 17, DLBCL 9) [8], Kikuchi et al. showed a 6-year EFS with 82% for 91 patients (BL 45, B-ALL 9, DLBCL 26, others 11) [10], and Tsurusawa et al. showed a 7-year EFS with 93% for 30 patients with DLBCL [9]. In addition, Lee et al. has recently shown a 5-year EFS with 95% for 61 patients (BL 46, DLBCL 15) [11]. However, the treatment duration of these studies was relatively long and the number of patients was small compared to the European and North American studies [1–6].

Here, we report on the results of the nation-wide large prospective study for children with B-NHL. The primary object was to evaluate the efficacy and safety of short-pulse intensive chemotherapy regimen designed by the Japanese Pediatric Leukemia/Lymphoma Study Group (JPLSG).

DOI 10.1002/pbc.24975
Published online 13 February 2014 in Wiley Online Library (wileyonlinelibrary.com).

PATIENTS AND METHODS

Study Design and Diagnostic Criteria

The B-NHL03 study was a prospective nonrandomized trial that investigated the efficacy and safety of short-pulse intensive chemotherapy in childhood B-NHL. The chief aim was to improve the outcomes of patients enrolled in the B-NHL03 study to the level of those of European and North American studies.

Additional Supporting Information may be found in the online version of this article.

[1]Advanced Medical Research Center, Aichi Medical University, Aichi, Japan; [2]Division of Pediatric Oncology, National Center for Child Health and Development, Tokyo, Japan; [3]Department of Pediatrics, Teikyo University, Tokyo, Japan; [4]Pediatric Hematology/Oncology, Yamagata University Hospital, Yamagata, Japan; [5]Department of Pediatrics, Japanese Red Cross Narita Hospital, Chiba, Japan; [6]Department of Pediatrics, Sapporo Hokuyu Hospital, Sapporo, Japan; [7]Clinical Research Center, National Center for Child Health and Development, Tokyo, Japan; [8]Clinical Research Center, National Hospital Organization Nagoya Medical Center, Nagoya, Japan; [9]Department of Nutrition and Health, Faculty of Psychological and Physical Science, Aichi Gakuin University, Aichi, Japan; [10]Department of Pathology, National Center for Child Health and Development, Tokyo, Japan; [11]Department of Pathology, School of Medicine, Kurume University, Kurume, Japan

Grant sponsor: Ministry of Health, Labor and Welfare of Japan; Grant number: H14, H15, H16, H17, H20, H23

Conflict of interest: Nothing to declare.

*Correspondence to: Masahito Tsurusawa, Advanced Research Center, Aichi Medical University, Nagakute, Aichi 480-11, Japan.
E-mail: mtsuru@aichi-med-u.ac.jp

Received 4 October 2013; Accepted 16 January 2014

The diagnosis of B-NHL was based on histopathology, immunocytochemistry, and cytogenetics. All histopathological specimens were first classified by the institutional pathologist and finally each of them were reviewed by a group of seven pathologists of a central pathological review committee according to WHO classification, that is, BL or Burkitt-like lymphoma (BLL), DLBCL, mediastinal large B-cell lymphoma (MLBCL), and mature B-cell neoplasm, NOS (not otherwise specified) [12]. A mature B-cell phenotype was primarily defined as positive for C20 and/(or) CD79a and negative for CD3 and terminal deoxynucleotidyl transferase. When an immunophenotype study was not available, specific translocations t(8;14)(q24;q32), t(2;8)(p11;q24), t(8;22)(q24;q11) at cytogenetic analysis were included. CNS involvement was diagnosed by the presence of one or more of the following: any blasts with FAB L3 morphology in CSF, isolated intracerebral mass, or intra-spinal extension. The clinical stage was defined by Murphy's classification [13].

Treatments

The treatment outline is shown in Figure 1 and chemotherapy regimens are shown in Table I. They were stratified into four treatment groups according to disease stage, tumor resectability and bone marrow/CNS involvement: Group 1 with all resected stage I/II, Group 2 with non-resected stage I/II, Group 3 with stage III & CNS-negative stage IV, and Group 4 with CNS-positive stage IV & B-ALL. All groups except Group 1 received a pre-phase therapy of prednisolone (PSL), vincristine (VCR), CPA and it (intrathecal) MTX to reduce tumor volume. As shown in Figure 1, Group 1 received two courses (1A × 2), Group 2 received 4 courses (2A × 2 + 2B × 2), Group 3 received 6 courses (3A × 4 + 3B × 2), and Group 4 received 6 courses (4A1 × 2 + 4A2 × 2 + 4B × 2), respectively. No patients received prophylactic cranial irradiation. Patients with CNS involvements received HDMTX (5 g/m^2) plus an extended it regimen (14 times), but no therapeutic cranial irradiation. The schedule of HDMTX administration was identical

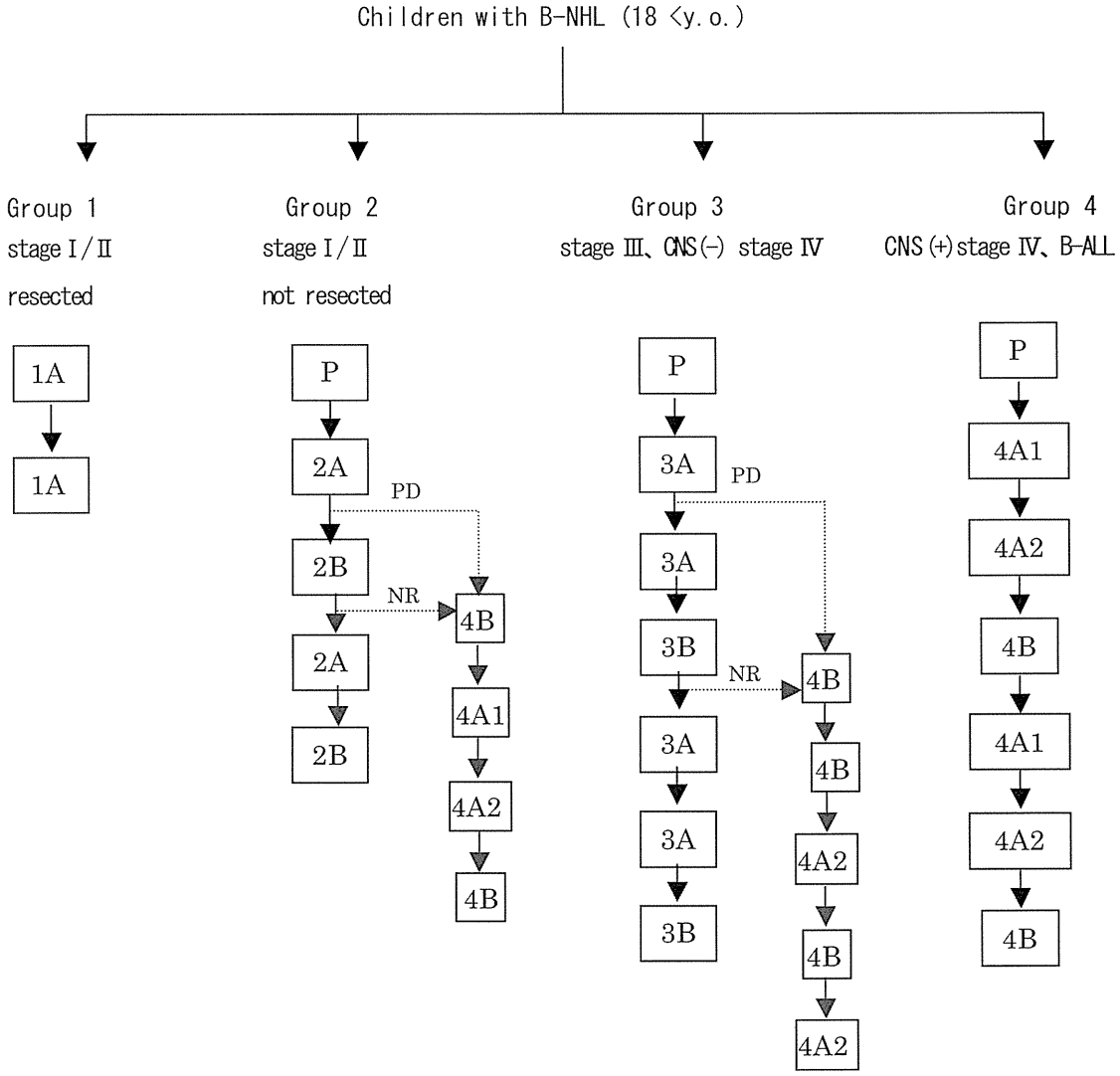

Fig. 1. Treatment framework of the B-NHL03 study. Patients were stratified into four treatment groups according to disease stage, tumor resectability, and BM/CNS involvement. All groups except Group 1 received pre-phase therapy. Group 1 received two courses of chemotherapy, Group 2 received 4 courses, Groups 3 and 4 received 6 courses, respectively. When patients in Group 2 or 3 did not achieve CR or CRu during the first 2 or 3 courses, they received salvage therapy consisting of 4B and 4A1/2 courses.

TABLE I. B-NHL03 Treatment Schedules

Regimen	Administration	Daily dose	Days
Pre-phase			
Prednisolone	Orally	30 mg and 60 mg/m^2	Days 1–3 and 4–7
Vincristine	IV	1 mg/m^2	Day 3
Cyclophosphamide	IV	150 mg/m^2	Days 4–6
Methotrexate	TIT	12 mg/m^2	Day 1, (4)[a]
Hydrocortisone	TIT	25 mg/m^2	Day 1, (4)[a]
Cytarabine	TIT	30 mg/m^2	Day (4)[a]
Regimen 1A			
Prednisolone	Orally	60 mg/m^2	Days 1–5
Methotrexate	IV	1 g/m^2	Day 1
Vincristine	IV	1.5 mg/m^2	Day 2
Cyclophosphamide	IV	250 g/m^2 × 2	Days 2–4
THP-adriamycin	IV	30 mg/m^2	Days 3, 4
Methotrexate	DIT	12 mg/m^2	Day 1
Hydrocortisone	DIT	25 mg/m^2	Day 1
Regimen 2A			
Same as 1A except for dexamethasone	Orally	10 mg/m^2	Days 1–7
Methotrexate	IV 24 hours with LV rescue	3 g/m^2	Day 1
Regimen 3A			
Same as 2A except for *t.i.t* at day 1			
Regimen 4A1			
Same as 3A except for methotrexate	IV 24 hours with LV rescue	5 g/m^2	Day 1
Methotrexate	TIT	12 mg/m^2	Day 1, (5),[a] 8
Hydrocortisone	TIT	25 mg/m^2	Day 1, (5),[a] 8
Cytarabine	TIT	30 mg/m^2	Day 1, (5),[a] 8
Regimen 4A2			
Same as 4A1 except for cyclophosphamide	IV	1 g/m^2	Days 4, 5
Regimen 2B			
Methotrexate	IV 6 hours	500 mg/m^2	Day 1
Cytarabine	cIV	150 mg/m^2	Days 1–5
Methotrexate	DIT	12 mg/m^2	Day 1
Hydrocortisone	DIT	25 mg/m^2	Day 1
Regimen 3B			
Same as 2B except for TIT at day 1, and cytarabine	cIV	150 mg/m^2	Days 1–6
Etoposide	IV	100 mg/m^2 × 2	Days 3–5
Regimen 4B			
Same as 3B except for without methotrexate, DIT at day 1 and TIT at day 8, and dexamethasone	Orally	10 mg/m^2	Days 1–7
Cytarabine	IV	2 g/m^2 × 2	Days 2–4
Etoposide	IV	150 mg/m^2	Days 2–5
Vincristine	IV	1.5 mg/m^2	Day 1

LV, leucovorin; IV, intravenous; cIV, continuous intravenous; DIT, double intrathecal; TIT, triple intrathecal. [a]For CNS positive patients.

to that of the B-NHL960 study [9]: HDMTX was administered for the first 24 hours, and 12 hours later, leucovorin (LV) 15 mg/m^2 was given orally every 6 hours, for a total of seven doses [9]. Blood MTX concentration was measured 24, 48, and 72 hours after the MTX administration. When patients showed delayed MTX clearance ($\geqq$0.2 μM after 72 hours), LV rescue was continued until MTX concentration level decreased to less than 0.2 μM.

Induction failure (IF) was defined as patients who did not achieve complete remission (CR) or unconfirmed remission (CRu) until the last evaluation time (before the second course of 2A in Group 2, before the third course of 3A in Group 3, before the second course of 4A1 in Group 4). When patients in Group 2 or 3 were evaluated to have progressive disease or no response during the first 2 or 3 courses, they received salvage therapy consisting of regimens 4B and 4A1/2. The cumulative dose of cytotoxic drugs for treatment groups was as follows: CPA 3 g/m^2, THP 120 mg/m^2 for Group 1; CPA 3.45 g/m^2, THP 120 mg/m^2 for Group2; CPA 6.45 g/m^2, THP 240 mg/m^2, VP16 0.6 g/m^2 for Group 3; CPA 7.45 g/m^2, THP 240 mg/m^2, VP16 1.2 g/m^2 for Group 4.

Statistical Analysis

Final statistical analyses were performed based on data obtained in June 2012. Overall survival (OS) was defined as the time between diagnosis and death from any causes, and EFS was defined as the time to first events defined as an occurrence of induction failure, relapse at any site, death from any causes, or second malignant neoplasm. For patients who did not experience an event, EFS was defined as the time to the last follow-up. Survival curves were prepared using the Kaplan–Meier method and standard errors (SEs) with the Greenwood formula. The significance of differences in survival outcomes was determined by means of the log-rank test.